Article

Activated PI3K Delta Syndrome-1 mutations cause neutrophilia in zebrafish larvae

Elworthy, Stone, Rutherford, Holly A., Prajsnar, Tomasz K., Hamilton, Noémie M., Vogt, Katja, Renshaw, Stephen A. and Condliffe, Alison M.

Activated PI3K Delta Syndrome-1 mutations cause neutrophilia in zebrafish larvae

Stone Elworthy[1], Holly A. Rutherford[1], Tomasz K. Prajsnar[1,2], Noémie M. Hamilton[1], Katja Vogt[1,3], Stephen A. Renshaw[1,*], Alison M. Condliffe[1,*]

[1]Department of Infection, Immunity and Cardiovascular Disease, University of Sheffield, Sheffield, UK
[2]Institute of Zoology, Jagiellonian University, Krakow, Poland
[3]Current address; School of Medicine, University of Central Lancashire, Preston, UK

*Corresponding authors, contributed equally

Keywords: APDS, zebrafish, PI3K-delta, Homology-directed gene editing, CRISPR, Cas12a, Cpf1, neutrophil, neutrophilia

Summary Statement

This study uses zebrafish embryos and homology-directed gene editing to investigate the effect of APDS1 disease mutations on innate immune cells; observing neutrophilia without defects in neutrophil differentiation or migration.

Abstract

People with Activated PI3 Kinase Delta Syndrome 1 (APDS1) suffer from immune deficiency and severe bronchiectasis. APDS1 is caused by dominant activating mutations of the *PIK3CD* gene that encodes the PI3 kinase delta (PI3Kδ) catalytic subunit. Despite the importance of innate immunity defects in bronchiectasis, there has been limited investigation of neutrophils or macrophages in APDS1 patients or mouse models. Zebrafish embryos provide an ideal system to study neutrophils and macrophages. Previous studies of zebrafish with strongly hyperactivated PI3 kinase activity due to Pten deficiency, revealed excessive production of immature neutrophils that fail to mature. We used CRISPR-Cas9 and CRISPR-

Cpf1, with oligo-nucleotide directed homologous repair, to engineer zebrafish equivalents of the two most prevalent human APDS1 disease mutations. These zebrafish *pik3cd* alleles dominantly cause excessive neutrophilic inflammation in a tail-fin injury model. They also exhibit total body neutrophilia in the absence of any inflammatory stimulus but have normal numbers of macrophages. Exposure to the PI3Kδ inhibitor CAL-101 reverses the total body neutrophilia. There is no apparent defect in neutrophil maturation or migration and tail-fin regeneration is unimpaired**.**

Introduction

Activated PI3 Kinase Delta Syndrome 1 (APDS1) is a complex syndrome of immune system defects (Angulo et al. 2013, Lucas et al. 2014, Lucas et al. 2016, Michalovich and Nejentsev 2018, Singh et al. 2020, Brodsky and Lucas 2021). Previous investigations of human APDS1 patients and mouse models have revealed T-cell and B-cell defects but it is currently unclear whether there are also neutrophil or macrophage defects (Brodsky and Lucas 2021).

APDS1 is caused by dominant gain of function mutations in the *PIK3CD* gene that encodes the PI3 kinase delta (PI3Kδ) catalytic subunit (p110δ) (Jou et al. 2006, Angulo et al. 2013, Lucas et al. 2014). PI3Kδ and its paralogues (PI3Kα and PI3Kβ), comprise the Class IA PI3 kinases (Burke and Williams 2015). These are each heterodimers of their respective catalytic domain proteins with a common regulatory domain protein (p85 encoded by *PIK3R*). In response to transmembrane receptor signalling, they phosphorylate the membrane phospholipid Ptdlns(4,5)P_2 to generate the second messenger Ptdlns(3,4,5)P_3. PtdIns(3,4,5)P_3 activates a downstream kinase cascade including AKT, that modulates mTOR and FOXO1, controlling differentiation, metabolism and proliferation (Burke and Williams 2015, Lucas et al. 2016, Nunes-Santos et al. 2019). The Ptdlns(3,4,5)P_3 phosphatases, PTEN and SHIP, provide a reverse activity crucial for overall function of the signalling pathway (Nishio et al. 2007, Choorapoikayil et al. 2014, Browning et al. 2015).

PI3Kδ is predominantly expressed in haemopoietic stem and progenitor cells (HSPCs) and leukocytes (Burke and Williams 2015). In human HSPCs, lymphocytes and neutrophils, *PIK3CD* expression is more abundant than the *PIK3CA* and *PIK3CB* paralogues (encoding

PI3Kα and PI3Kβ) (Xie et al. 2021). Human monocytes and myelocytes strongly express *PIK3CD* along with *PIK3CB* (Xie et al. 2021).

PI3Kδ has diverse roles in modulating the differentiation and activity of different leukocytes (Okkenhaug et al. 2002, Lucas et al. 2016, Nunes-Santos et al. 2019). During emergency granulopoiesis in response to bacterial infection, PI3Kδ activity induces HSPCs to proliferate and differentiate to provide extra neutrophils (Kwak et al. 2015, Mistry et al. 2019). To provide adaptive immunity, PI3Kδ activity in B cells and T cells needs to be fine-tuned for various stages of differentiation. This level of PI3Kδ activity is set by signalling from antigen receptors, co-stimulatory receptors, cytokine receptors and growth factor receptors (Lucas et al. 2016, Nunes-Santos et al. 2019). Neutrophil migration and production of reactive oxygen species is controlled by PI3Kγ (PI3 kinase class 1B) (Hirsch et al. 2000, Li et al. 2000, Sasaki et al. 2000, Hannigan et al. 2002, Yoo et al. 2010). A role for PI3Kδ in these processes has also been implicated but is less clearly established (Sadhu et al. 2003, Condliffe et al. 2005, Liu et al. 2007, Sapey et al. 2014).

Studies of APDS1 patients identified B cell and T cell defects resulting from dysregulated excessive PI3Kδ activity (Angulo et al. 2013, Lucas et al. 2014). The most prevalent causative APDS1 mutation is E1021K in the p110δ catalytic domain, whilst the second most prevalent is E525K in the helical domain. E1021K is predicted to enhance membrane association whilst E525K is predicted to perturb regulatory interactions with the p85 regulatory partner (Dornan et al. 2017, Michalovich and Nejentsev 2018). These alleles lower the PI3K activation threshold and mirror oncogenic mutations at equivalent positions of PI3Kα. The PI3Kδ inhibitor Leniolisib offers a promising treatment option (Rao et al. 2017). Mouse models of the E1021K mutation have further elucidated the mechanisms underlying the B cell and T cell defects (Avery et al. 2018, Stark et al. 2018, Wray-Dutra et al. 2018) and more generally, the role of PI3Kδ in lymphocytes. In addition to disrupting adaptive immunity, aberrant PI3Kδ signalling in such mice expands a subpopulation of B cells that increase immediate susceptibility to *Streptococcus pneumoniae* infection (Stark et al. 2018).

Severe inflammatory airway damage (termed bronchiectasis) is a prominent APDS1 symptom and possibly suggestive of additional defects of the innate immune system (Condliffe and Chandra 2018). However, there has been limited investigation of neutrophils and macrophages in APDS1 patients or mouse models (Chiriaco et al. 2017, Stark et al. 2018).

Zebrafish embryos provide an excellent model system for investigating neutrophil and macrophage development and function. The consequence of hyperactive PI3K signalling on myelopoiesis has previously been studied using zebrafish lacking PTEN (Choorapoikayil et al. 2014). Lack of PTEN induces an expansion of HSPCs and, although definitive myeloid and lymphoid lineages enter early stages of development, differentiation fails to complete (Choorapoikayil et al. 2014). Neutrophils from the primitive wave of myelopoiesis fully differentiate and are more numerous, whilst neutrophils from the definitive wave differentiate to the point of expressing *mpx* but not to having granules that can be stained with Sudan-black dye (Choorapoikayil et al. 2014).

The zebrafish *PIK3CD* orthologue, *pik3cd* has been characterised as a *runx1*-dependent, early marker of HSPCs (Bonkhofer et al. 2019). Expression of *pik3cd* is observed, both in nascent HSPCs as they differentiate from the dorsal aorta, and in the posterior blood island (Bonkhofer et al. 2019). Single-cell mRNA sequencing studies of zebrafish larval stages and adults also show extensive expression of *pik3cd* in neutrophils, macrophages and HSPCs along with extensive expression of *pik3cg* and *pik3cb* encoding zebrafish PI3Kγ and PI3Kβ (Athanasiadis et al. 2017, Tang et al. 2017, Farnsworth et al. 2020).

We have used homology-directed gene editing of zebrafish *pik3cd*, to generate the first zebrafish hyperactivating PI3Kδ APDS1 models and investigate possible primary defects in neutrophils or macrophages at a developmental stage prior to the development of the zebrafish adaptive immune system.

Results

Homology-directed CRISPR-Cas9 knock-in of a zebrafish model for *PIK3CD*^{E525K}

The zebrafish genome sequence assembly (GRCz11) has one *pik3cd* gene encoding an ortholog of the human *PIK3CD*. DNA sequence database searching confirms that the closest *pik3cd* paralogues are genes encoding PI3Kβ, γ and α catalytic subunits (TBLASTN search of GRCz11 with human PIK3CD protein sequence). This indicates that zebrafish *pik3cd* could provide a suitable model for investigating mechanisms of human APDS1.

Zebrafish *pik3cd* has extensive ammino acid sequence homology to human *PIK3CD*, with conservation of the residues mutated in the two most prevalent APDS1 disease-causing mutations E1021K and E525K. We sought to mimic these by using gene editing to generate zebrafish *pik3cd* alleles with the equivalent E1017K and E525K mutations.

Single strand oligonucleotide (ssODN) directed gene editing with CRISPR-Cas9 has recently become established as a method for knocking-in point mutations in the zebrafish genome (Prykhozhij and Berman 2018, Prykhozhij et al. 2018). Editing efficiency relies on having an efficient CRISPR cleavage site within 10bp of the intended mutation (Prykhozhij and Berman 2018). Searching with CRISPR-Cas9 design software revealed that the zebrafish *pik3cd* E1017 site (equivalent to the human *PIK3CD* E1021) lacks nearby potential CRISPR-Cas9 cleavage sites. We were, however, able to design a guide RNA for a potential cleavage site 8bp from the *pik3cd* E525 site Fig.1A,B). These practicalities caused us to first direct our efforts towards the *pik3cd* E525 site despite its lower clinical significance.

To knock-in the *pik3cd*^{E525K} mutation, we followed recommendations (Prykhozhij et al. 2018), designing an asymmetric, 140mer, template strand, ssODN donor, with two phosphothioates at each end. The ssODN donor sequence had two further silent point mutations in addition to the E525K causing point mutation (Fig.1A). These were designed for three joint purposes- to prevent the CRISPR-Cas9 recutting after a successful edit; to create a primer binding site for sensitive PCR detection of edited genomic DNA; and to create an Apo1 restriction site for robust genotyping once a mutant allele was established (Fig.1A,D,E,F). The intended edited sequence was checked through intron splicing predictive software to avoid inadvertently perturbing mRNA splicing.

Zebrafish embryos, at one cell stage, were injected with a mix of the donor ssODN, Cas9 protein, generic tracrRNA oligonucleotide and guide crRNA oligonucleotide. As a negative control, sibling embryos were left uninjected or injected with donor ssODN alone. At three days of development (3dpf) some individual embryos were sacrificed and analysed by PCR with a primer specific for the intended genome edit together with a primer external to the donor ssODN sequence region (Fig.1A,B,C,D). Agarose gel electrophoresis revealed robust amplification of the expected 103bp amplicon from each of the embryos injected with CRISPR-Cas9 and donor ssODN but not those with donor alone (Fig.1D). In addition to the expected 103bp amplicon, embryos injected with CRISPR-Cas9 and donor, also gave multiple lower mobility amplicons that differed between embryos. Reduced electrophoretic mobility is consistent with the indel types identified in previous reports of ssODN knock-in leading to integrated fragments of donor and partially mismatched hybrid amplicons (Boel et al. 2018, Prykhozhij et al. 2018). These injected embryos are interpreted as likely to be genetic mosaic, with a mix of unaltered cells, some cells with alleles involving indels together with the edit, and some cells with the intended edit (Boel et al. 2018, Prykhozhij et al. 2018).

Injected embryos (G0) were raised to adulthood and nine adults outcrossed to identify and isolate a line with the intended *pik3cd* edit. From each outcross, 24 embryos were lysed separately in individual wells in a 96well plate. As a preliminary screen, the edit-specific PCR test was conducted on three pools of eight embryo lysates from each outcross. Lysates from positive pools were then retested individually (Fig.1E) and, if positive, a 152bp PCR product across the edit region was sequenced. When that sequence had the intended edit, overlapping 518bp and 658bp PCR products were sequenced spanning the edit.

This analysis indicated that four of the nine tested G0 adults did not exhibit germline transmission of the *pik3cd* edit; three G0 adults transmitted edits combined with unwanted indels whilst two G0 adults transmitted the intended *pik3cd*^{E525K} edit. Embryos were raised from one of these fish and *pik3cd*^{E525K} adults identified by edit-specific PCR from fin-clip lysates. Sequence from PCR amplicons covering 891bp across the edit region confirmed the integrity of the edit in the established line (Fig.1B,G). This line has the allele designation *pik3cd*^{sh673} but for clarity here will be referred to as *pik3cd*^{E525K}.

When progeny from *pik3cd*$^{E525K/+}$ in-crosses were raised, no obvious external phenotype was apparent and genotypes of the resulting adults followed the expected Mendelian ratio with 20 *pik3cd*$^{+/+}$, 31 *pik3cd*$^{E525K/+}$ and 16 *pik3cd*$^{E525K/E525K}$ (Chi-squared test P=0.65).

Homology directed CRISPR-LbCpf1 knock-in of a zebrafish model for *PIK3CD*^{E1021K}

Although the zebrafish *pik3cd* E1017 site (equivalent to the human *PIK3CD* E1021) lacks nearby potential CRISPR-Cas9 cleavage sites, it is 3bp from a predicted CRISPR-LbCpf1 cleavage site. We made use of this alternative CRISPR technology for ssODN directed gene editing. We broadly followed the method of (Moreno-Mateos et al. 2017, Fernandez et al. 2018) but with a crRNA guide oligo with 5' and 3' extensions (Bin Moon et al. 2018, Park et al. 2018) (Fig.2A). A 142mer, symmetrical, non-template strand, knock-in donor ssODN was designed with two phosphothioates at each end. In addition to the point mutation causing E1017K, four additional silent point mutations were included (Fig.2B). As with the E525K strategy, these were designed to prevent the CRISPR recutting and to facilitate allele identification whilst avoiding inadvertently perturbing mRNA splicing (Fig.2B,C,D,E,G).

LbCpf1 protein was preincubated with guide crRNA before addition of donor ssODN and injected into one cell stage zebrafish embryos. At 3dpf, some individual embryos were sacrificed and analysed by PCR with a primer specific for the intended genome edit together with a primer external to the donor ssODN sequence region (Fig.2B,C). Agarose gel electrophoresis revealed robust amplification of the expected 113bp amplicon from each of the embryos injected with CRISPR-LbCpf1 and donor ssODN but not from uninjected controls (Fig.2D). One of the injected embryos also gave an additional lower mobility amplicon. As with the *pik3cd*^{E525K} knock-in, these injected embryos are interpreted as likely to be genetic mosaic, containing some cells with alleles involving indels together with the edit.

Injected (G0) embryos were raised to adulthood and 51 adults outcrossed to identify and isolate a line with the intended *pik3cd* edit. From each outcross, twenty-four embryos were lysed separately in individual wells in a 96well plate. As a preliminary screen, the edit-specific PCR test was conducted on three pools of eight embryo lysates from each outcross.

Edit-specific PCR amplification was observed for 19 out of the 51 G0 outcrosses. Lysates from positive pools were then retested individually and, if positive, a 332bp PCR product across the edit region was sequenced.

In some cases, either the edit-specific test PCR or the PCR spanning the edit region gave amplicons with lower-than-expected electrophoretic mobility (Fig.2E,F). Additionally, some embryos identified with the allele specific test PCR subsequently gave wild type sequence from the 322bp PCR product spanning the edit region. Nevertheless, we did identify one adult transmitting a *pik3cd*^{E1017K} allele with the correct sequence across the 332bp region (Fig.2E). Two hundred and fifty-four embryos from this fish were raised to adulthood and 22 were identified as *pik3cd*^{E1017K} by edit-specific PCR from fin-clip lysates. The 332bp PCR amplicon across the edit region was sequenced to confirm the integrity of the edit in the established line (Fig.2C,H). This line has the allele designation *pik3cd*^{sh674} but for clarity here will be referred to as *pik3cd*^{E1017K}.

When progeny from a *pik3cd*$^{E1017K/+}$ in-cross were raised, no obvious external phenotype was apparent and genotypes of the resulting adults followed the expected Mendelian ratio with seven *pik3cd*$^{+/+}$, 13 *pik3cd*$^{E1017K/+}$ and six *pik3cd*$^{E1017K/E1017K}$ (Chi-squared test P=0.96).

pik3cd$^{E1017K/+}$ embryos and *pik3cd*$^{E525K/+}$ embryos exhibit increased neutrophilic inflammation following tail-fin injury

Human patients with APDS1 are heterozygous for an activating *PIK3CD* mutant allele. We investigated whether our zebrafish *pik3cd* knock-in mutations similarly exhibited a phenotype when heterozygous with a wild type *pik3cd* allele. We used an established embryo tail-fin injury assay to investigate whether either of our *pik3cd* knock-in mutants influenced the inflammatory response (Lieschke et al. 2001, Renshaw et al. 2006) (Fig3.A).

Heterozygous carriers of the *pik3cd*^{E1017K} or *pik3cd*^{E525K} alleles were outcrossed to fish with the fluorescent neutrophil marker transgene *TgBAC(mpx:gfp)i114*. This allowed us to blindly compare sibling embryos that were either heterozygous for the *pik3cd* mutation, or fully wild

type (wt) (in the expected Mendelian 1:1 ratio). At 3dpf, embryos were injured, and fluorescent neutrophils were serially counted at the wound site from two hours post injury (hpi) until 24hpi, spanning the normal inflammation and resolution time course. The embryos were then genotyped, by PCR across the *pik3cd* mutation site and Apo1 digestion.

Compared to their wt siblings, the embryos with either *pik3cd*$^{E1017K/+}$ or *pik3cd*$^{E525K/+}$, had increased neutrophil counts at the wound site, not only at the 4hpi peak inflammatory time point but also throughout the time course (Fig3.B,C,D,E).

pik3cd$^{E1017K/+}$ embryos and *pik3cd*$^{E525K/+}$ embryos have increased total body neutrophils

Following our observations from the tail-fin injury assay, we sought to establish whether *pik3cd*$^{E1017K/+}$ and *pik3cd*$^{E525K/+}$ embryos simply had more neutrophils, even in the absence of an inflammatory stimulus. Sibling embryos from a *pik3cd*$^{E1017K/+}$ outcross with *TgBAC(mpx:gfp)i114* were analysed by light sheet microscopy at 3dpf to count total body neutrophils and then genotyped (Fig.4A,B). Similarly, embryos from a *pik3cd*$^{E525K/+}$ outcross were analysed at 3dpf with spinning-disk microscopy and at 2dpf with light sheet microscopy (Fig.4C,D,E). In each case, the embryos with *pik3cd* knock-in mutation had higher total body neutrophil numbers than their wt siblings.

We also investigated whether *pik3cd*$^{E1017K/+}$ adult zebrafish had an increased proportion of neutrophils in their whole kidney marrow (WKM, the zebrafish adult haemopoietic tissue). Fish from *pik3cd*$^{E525K/+}$ outcrosses with *TgBAC(mpx:gfp)i114* were raised together until eight months old. Flow cytometry of their WKM was used to identify leukocytes and precursors (Traver et al. 2003) and count the proportion from that cell population expressing the neutrophil marker *TgBAC(mpx:gfp)i114*. This analysis did not detect a significant difference between the *pik3cd*$^{E525K/+}$ adults and their wt siblings (Fig S1).

The PI3Kδ inhibitor CAL-101 reduces neutrophil numbers

Since the *pik3cd* knock-in mutations were expected to act by increasing PI3Kδ activity, we tested whether the neutrophilia phenotype was counteracted by exposure to the specific PI3Kδ inhibitor CAL-101 (Idelalisib) (Lannutti et al. 2011). Sibling embryos from a

pik3cd$^{E1017K/+}$ outcross with *TgBAC(mpx:gfp)i114* were exposed to CAL-101 from 24hpf until 48hpf and then analysed by spinning disk microscopy and genotyped. CAL-101 exposure reduced neutrophil numbers both for the *pik3cd*$^{E1017K/+}$embryos and their wt siblings (Fig.4D,E).

Excessive neutrophilic inflammation is also observed after the definitive wave and the neutrophils are differentiated

The neutrophilia we observed with our *pik3cd* knock-in mutants, suggested comparison with previous findings from zebrafish lacking PTEN. It has previously been shown that *ptena*$^{-/-}$*;ptenb*$^{-/-}$ double mutants have excessive *mpx*-expressing neutrophils, both from the primitive and the definitive wave. However, the *ptena*$^{-/-}$*;ptenb*$^{-/-}$ definitive wave neutrophils fail to fully differentiate and so, at 5dpf, a large proportion of tail neutrophils are not stainable with Sudan black dye (Choorapoikayil et al. 2014).

We used a 5dpf tail-fin injury assay to analyse definitive wave neutrophils in *pik3cd*$^{E1017K/+}$ and *pik3cd*$^{E525K/+}$ larvae. Sibling larvae from a *pik3cd*$^{E1017K/+}$ or *pik3cd*$^{E525K/+}$ outcross with *TgBAC(mpx:gfp)i114* were subjected to a minor tail-fin injury at 5dpf. The larvae were fixed at 2hpi, stained with Sudan black dye and imaged to identify Sudan black stained and *TgBAC(mpx:gfp)i114* neutrophils at the wound region (Fig.5A). Genotyping after analysis, showed that the mutant larvae had excessive, Sudan black stained, neutrophils at the wound. Irrespective of *pik3cd* genotype, there were very few *TgBAC(mpx:gfp)i114* neutrophils not stained with Sudan black (Fig.5B,C).

***pik3cd*$^{E1017K/+}$ embryos have unaltered total body macrophage counts and unaltered susceptibility to a *Staphylococcus aureus* infection model**

We investigated whether the observed increase in total body neutrophils was accompanied by any alteration in total body macrophage numbers. We used the fluorescent macrophage nuclear marker transgene *Tg(mpeg1.1:NLS-clover)sh616*. Sibling embryos from a *pik3cd*$^{E1017K/+}$ outcross with *Tg(mpeg1.1:NLS-clover)sh616* were analysed by light sheet microscopy at 2dpf to count total body macrophages and then genotyped. We observed no

difference in the total body macrophage numbers between the *pik3cd*$^{E1017K/+}$ embryos and their wt siblings (Fig.6A,B).

Innate immune cell function is known to be critical for resistance to the pathogen *Staphylococcus aureus* in the circulation of larval zebrafish (Prajsnar et al. 2008, Prajsnar et al. 2012). We tested whether the *pik3cd*$^{E1017K/+}$ mutation altered susceptibility to such infection. Sibling 30hpf embryos from a *pik3cd*$^{E1017K/+}$ outcross were intravenously injected with 1500 colony forming units of *Staphylococcus aureus*. Dead and dying embryos were collected over the following 90 hours and then genotyped, along with all those still surviving at the end. The survival of the *pik3cd*$^{E1017K/+}$ larvae was unaltered from their wild type siblings with the expected approximately 50% mortality (Fig.6C).

pik3cd$^{E1017K/+}$ and *pik3cd*$^{E525K/+}$ embryos have normal tail-fin regeneration

In some contexts, excessive neutrophilic inflammation is implicated in impaired regeneration after injury (Tsarouchas et al. 2018, Bernut et al. 2020). We investigated whether there was also such an effect from the excessive neutrophilic inflammation we observed after tail-fin injury in our *pik3cd* knock-in mutants. At 3dpf, tail-fins of *pik3cd*$^{E1017K/+}$ or *pik3cd*$^{E525K/+}$ embryos and their wt siblings were injured and then allowed to regenerate for two days before imaging, measurement, and genotyping. Equally extensive areas of tail-fin regenerated in the mutant embryos and their wt siblings (Fig.7A,B,C).

Neutrophil Il-1β plays an important role mediating the influence of neutrophilic inflammation on regeneration (Tsarouchas et al. 2018). The *TgBAC(il1b:EGFP)sh445* reporter has previously been shown to be transiently upregulated in neutrophils after a 3dpf tail fin injury (Ogryzko et al. 2019). We used this assay to compare expression levels between *pik3cd*$^{E1017K/+}$ embryos and their wild-type siblings. Embryos were fixed three hours after injury and stained for myeloperoxidase activity to identify neutrophils. Using spinning disk microscopy, GFP fluorescence was measured in neutrophils and the embryos were genotyped. This analysis indicates that each neutrophil in *pik3cd*$^{E1017K/+}$ embryos had similar Il-1β expression as in the wild type siblings (Fig.7D,E).

pik3cd$^{E1017K/+}$ embryos have normal neutrophil migration

PI3K signalling is known to direct neutrophil migration (Liu et al. 2007, Nishio et al. 2007, Yoo et al. 2010) and inhibition of PI3Kδ or PI3Kγ restored migratory accuracy exhibited by neutrophils from healthy elder volunteers and COPD patients, linking increased constitutive PI3K activity with inaccurate neutrophil migration and potentially enhanced bystander damage (Sapey et al. 2011, Sapey et al. 2014). This raised the possibility that our *pik3cd* knock-in mutants might exhibit aberrant neutrophil migration. We used a *TgBAC(mpx:gfp)i114* tail-fin injury inflammation model to track neutrophil migration in 3dpf *pik3cd*$^{E1017K/+}$ embryos and their wt siblings. Widefield time-lapse video microscopy allowed neutrophil migration to be tracked over a six-hour time-course following a minor tail-fin needle injury (Fig.8A). Videos of neutrophils that migrated to the injury site were used to analyse the neutrophil migration paths; and the embryos genotyped. Consistent with our other observations, there were more neutrophils in the *pik3cd*$^{E1017K/+}$ embryos than in their wt siblings. However, no difference was detected for the neutrophil migration path speeds or meandering index of the two genotypes (Fig.8B,C,D,E).

Discussion

Zebrafish gene editing to recapitulate human disease alleles has recently become an accessible approach, thanks to CRISPR and ssODN technology (Prykhozhij and Berman 2018). CRISPR-Cas9 and CRISPR-LbCpf1 have differing DNA sequence requirements, which widens the scope of this method (Moreno-Mateos et al. 2017, Bin Moon et al. 2018). We had a favourable experience in using Cas9 to generate the *pik3cd*^{E525K} allele and LbCpf1 to generate the *pik3cd*^{E1017K} allele and would recommend either technology, depending on the DNA target site.

Our priority was to construct our *pik3cd* knock-in lines. During the procedure, we did not investigate the numerous instances where preliminary analysis of putative edited alleles failed to confirm a correct edit. The fish we used for mutagenesis and screening were not pre-screened to ensure that they were isogenic around the targeting site. Consequently, pre-existing polymorphisms, that interfered with PCR or sequencing, may have caused us to miss some correctly edited alleles. The underlying knock-in efficiency may therefore have been

higher than the overall efficiency we achieved. Using a stock of fish isogenic at the edit region, might be preferable for any future gene editing projects. It is also difficult to use our results to compare the relative editing efficiency of Cas9 and LbCpf1. However, both proved to be adequate for convenient use.

This study used embryos from out-crosses of fish heterozygous for the *pik3cd* knock-in mutations, and then genotyped the embryos after analysis. That enabled, internally controlled, blinded, comparison between mutant and wildtype sibling embryos. For future work, requiring bulk analysis or rapid screening, it may be more convenient to use clutches entirely of mutant embryos from a homozygous parent.

Human APDS1 patients are heterozygous for activating *PIK3CD* alleles as with our zebrafish models. Both of our *pik3cd* knock-in alleles exhibited the same dominant neutrophilia phenotype. The only correlate for this that we are aware of from human APDS1 patients, is a single case of bone marrow granulomatous hyperplasia (Lu et al. 2021). Previous studies of human APDS1 patients and mouse *Pikcd*$^{E1020K/+}$ models did not report neutrophilia (Angulo et al. 2013, Lucas et al. 2014, Avery et al. 2018, Stark et al. 2018). It is possible that if there is a comparable effect, from activated *pik3cd* mutations in mammals, it might be obscured by a confounding influence of adaptive immune system defects. Also, the small size and transparency of zebrafish embryos facilitates total body examination of neutrophils and macrophages whilst mammalian investigations typically analyse blood, which may not always reflect total body cell numbers. These same caveats apply to our analysis of adult zebrafish marrow that similarly did not detect an effect from the activated *pik3cd* mutation. Potentially though, the mechanism causing the neutrophilia in larvae could be developmental stage specific.

The neutrophilia phenotype of our knock-in alleles was counteracted by the PI3Kδ inhibitor CAL-101 (Idelalisib), which also reduced neutrophil numbers in wt embryos. Neutropenia is a common side effect for human patients treated with Idelalisib for haematological malignancies (de Weerdt et al. 2017). The identical phenotype observed in both *pik3cd* APDS1 knock-in alleles plus the reversal with a clinical PI3Kδ inhibitor gives confidence

that the neutrophilia is indeed due to PI3Kd hyperactivation, with potential relevance to the human disease.

The neutrophilia phenotype of our knock-in alleles is consistent with mechanisms for emergency granulopoiesis in mice (Kwak et al. 2015, Mistry et al. 2019). Emergency granulopoiesis generates extra neutrophils in response to inflammatory stimuli such as bacterial infection or experimental exposure to bacterial lipopolysaccharide (LPS). In response to this inflammatory stimulus, PI3Kδ-dependent AKT phosphorylation, in haemopoietic stem cells (HSCs) and bone marrow stromal cells (BMSCs), causes proliferation of progenitors and rapid differentiation to neutrophils (Kwak et al. 2015, Mistry et al. 2019). Emergency granulopoiesis has also been described in zebrafish embryos where bacterial infection causes neutrophilia without an accompanying increase in macrophages (Hall et al. 2012). We observe that same pattern with our *pik3cd* knock-in alleles. Altogether, this may indicate that our *pik3cd* knock-in alleles constitutively induce a state analogous to emergency granulopoiesis.

The role of PI3Kδ during emergency granulopoiesis invites comparison to the role of PI3Kδ in acute myeloid leukaemia (AML). AML is an uncontrolled proliferation of abnormal myeloid progenitors. Intriguingly, although human AML blasts exhibit constitutive PI3Kδ activity, it is not associated with *PIK3CD* mutations (Cornillet-Lefebvre et al. 2006, Darici et al. 2020). Mice with HSPCs lacking PTEN (Yilmaz et al. 2006, Zhang et al. 2006), or with hyper-active ATK (Kharas et al. 2010) develop AML. Zebrafish larvae lacking PTEN similarly exhibit an expansion of HSPCs and, although definitive myeloid and lymphoid lineages enter early stages of development, differentiation fails to complete (Choorapoikayil et al. 2014).

There are notable contrasts between our *pik3cd* knock-in mutants and zebrafish lacking PTEN. Zebrafish lacking PTEN are not viable and are deformed by 5dpf, whilst our *pik3cd* knock-in mutants are adult viable. Zebrafish lacking PTEN (due to $ptena^{-/-};ptenb^{-/-}$ mutations) have excessive fully differentiated neutrophils from the primitive wave, whilst definitive wave neutrophils differentiate to the point of expressing *mpx* but not to having granules that

can be stained with Sudan-black dye (Choorapoikayil et al. 2014). Consequently, at 5dpf, zebrafish lacking PTEN have excessive Sudan-black stainable neutrophils in anterior regions but a pronounced deficit in the tail (Choorapoikayil et al. 2014). By contrast, our *pik3cd* knock-in mutants exhibited excessive neutrophilic inflammation in the tail at 5dpf and the neutrophils showed no reduction in Sudan black staining. Presumably our knock-in mutants had sufficient PI3K signalling to share the *ptena*$^{-/-}$;*ptenb*$^{-/-}$ phenotype of expanded early steps of myelopoiesis but not so much to stall later differentiation. The more subtle and restricted phenotypes of our *pik3cd* knock-in mutants offer further opportunities for investigating the role of PI3K signalling in haemopoiesis.

Recurrent bacterial respiratory infections are a feature of APDS1. Studies using genetic mosaic *Pik3cd*$^{E1020K/+}$ mice found that increased susceptibility to *Streptococcus pneumoniae* infection was attributable to lymphocyte defects (Stark et al. 2018). Zebrafish larvae provide an infection model dependent on macrophages and neutrophils, prior to the development of functional lymphocytes (Prajsnar et al. 2008, Prajsnar et al. 2012). We found *pik3cd*$^{E1017K/+}$ larvae had unaltered susceptibility to the *Staphylococcus aureus* circulation infection model. This suggests that their macrophages and neutrophils retain bactericidal capability, in accord with the previous mouse findings.

Despite having excessive neutrophilic inflammation, our *pik3cd*$^{E525K/+}$ embryos were not defective in tailfin regeneration after injury. This contrasts with other examples where neutrophilic inflammation is associated with reduced regeneration. Zebrafish *runx1*$^{-/-}$ mutants have reduced neutrophils and accelerated regeneration after tail-fin injury (Li et al. 2012). Similarly, neutrophil depleted mice have accelerated wound closure (Dovi et al. 2003). In a zebrafish larval spinal cord injury model, I-1β produced by neutrophils impeded regeneration (Tsarouchas et al. 2018). We observed that the fluorescence intensity of the *TgBAC(il1b:EGFP)sh445* reporter in each neutrophil appeared as strong in *pik3cd*$^{E1017K/+}$ embryos, indicating that the neutrophils retained that inflammatory function in the mutant. The increased neutrophilic inflammation in our *pik3cd*$^{E525K/+}$ and *pik3cd*$^{E1017K/+}$ embryos after tail-fin injury was at a similar level to that reported for zebrafish *cftr*$^{-/-}$ (cystic fibrosis transmembrane conductance regulator) mutant embryos (Bernut et al. 2020). However, *cftr*$^{-/-}$ mutant embryos exhibit a pronounced reduction in tail-fin regeneration, alleviated by

reducing neutrophils (Bernut et al. 2020). Differences in the regenerating tissue and/or the activation state of the neutrophils may account for this difference in regeneration between *cftr*$^{-/-}$ and our activating *pik3cd* mutations.

PI3K activity is a key determinant of neutrophil motility (Sasaki et al. 2000, Liu et al. 2007, Nishio et al. 2007, Yoo et al. 2010). Excessive PI3K activity in human neutrophils (from chronic obstructive pulmonary disease (COPD) patients or healthy volunteers age >65) is associated with defective chemotactic directionality (Sapey et al. 2011, Sapey et al. 2014). We considered it plausible that aberrant PI3Kδ might interfere with neutrophil migration in our *pik3cd*$^{E1017K/+}$ embryos. However, they exhibited apparently normal neutrophil motility in response to a tailfin injury. Presumably the required localised balance between PI3 kinase and phosphatase activities is still maintained to allow normal migration. Alternatively, a subtle defect may have been beyond the sensitivity of our assay.

It is not immediately obvious whether the neutrophilia phenotype of our knock-in mutants relates to the disease aetiology of APDS in human patients. However, insights into PI3Kδ signalling, with medical relevance beyond treatment of APDS itself, have come from the investigations into APDS mutations in humans and mice. The zebrafish knock-in mutations, described here, add significantly to this, and provide a model system suitable for further studies.

Materials and Methods

Zebrafish strains, maintenance and pharmacological treatment

Zebrafish were maintained in accordance with UK Home Office regulations. Embryos were obtained by pair mating and incubated at 28^{o}C in E3 medium (without methylene blue if used for imaging or infection assays). *TgBAC(mpx:gfp)i114* is previously described (Renshaw et al. 2006). *Tg(mpeg1.1:NLS-clover)sh616* was isolated by outcrossing from the *Tg(mpeg1.1:NLS-clover)* stock described in (Bernut et al. 2019). *Tg(mpeg1.1:NLS-clover)sh616* exhibits Mendelian transmission, indicating that it is a single insertion. To aid imaging for some experiments, embryos were either exposed to 200μM 1-phenyl-2-thiourea

from 24hpf or had the *mitfa*^{w2} melanophore deficiency (Lister et al. 1999). Anaesthesia to allow handling, inspection or imaging used immersion in 0.164mg/ml Tricaine.

For CAL-101 exposure, dechorionated 24hpf embryos were immersed in 25µM CAL-101 (Selleckchem) in 1% DMSO in E3 at 25 embryos per 8ml volume glass petri dish. To make the immersion mixture, CAL-101 dissolved in DMSO was added to vortexing E3 in a glass tube. Controls were similarly immersed in 1% DMSO in E3.

CRISPR ssODN directed knock-in

BDGP (Reese et al. 1997), ESEfinder (Smith et al. 2006) and HSF (Desmet et al. 2009) were used to screen against perturbation of predicted splicing when designing knock-in mutations.

Knock-in of the *pik3cd*^{E525K} allele followed (Prykhozhij et al. 2018). A CRISPR-Cas9 target site was identified using SSC (Xu et al. 2015) and CHOPCHOP (Labun et al. 2016). One cell stage embryos were injected with 1nl of a mix of 1µM custom phosphorothioated (*) Ultramer oligonucleotide 5'a*g*gtctttgcttctaaaataatggtttgttgatggattgaattgttgtagcaccagaagctgaaagagattgtggacaataaaaactccaccgaattcttcaaggatgagaaggagctgttgtggaagctgcgagagga*g*3' (IDT), 2µM Cas9 Nuclease S.pyogenes (NEB), 20µM tracrRNA (Merck) and 20µM custom crRNA (with spacer 5'cucauccucaaagaacucgg3') (Merck) and 0.05% phenol red (Merck).

Knock-in of the *pik3cd*^{E1017K} allele broadly followed (Bin Moon et al. 2018, Fernandez et al. 2018, Park et al. 2018). The CRISPR-Cpf1target site was identified using DeepCpf1 (Kim et al. 2018). 1µl of 200µM custom RNA oligo 5'uagguaauuucuacuaaguguagauaggtcaagtttaatgaagctuuuuuuuu3' (Merck), 0.2µl of 10xNEB buffer 2.1 and 0.5µl of 100µM Lba Cas12a (Cpf1) (NEB) were mixed and incubated 10min 25^{o}C; then added to 0.3µl 0.5% phenol red (Merck) and 1µl 3µM custom phosphorothioated (*) Ultramer oligonucleotide 5'g*t*cacaggactctttggcactggggaaatcggaggaggaagcactgaagaactttaaggtcaaattcaacaaagctctacgagagagttggaagaccaaggtgaactggatgatgcacacatttgccaaagataacagata*a*3' (IDT). One cell stage embryos were injected with 1nl of the resulting mix.

PCR, genotyping and sequencing

PCR primers were designed with Primer3 (Untergasser et al. 2012) and SnapGene software was used for molecular biology strategy and analysis.

Each 20µl PCR reaction used 1µl of embryo lysate or 0.5µl of adult fin-clip lysate (prepared by 30min 98^{o}C incubation in 50µl, 25mM KOH, 200µM EDTA, vortexing, neutralisation by addition of 50µl 40mM Tris HCl and centrifugation to precipitate debris). PCRs used FIREPol Master Mix (Solis BioDyne) with touch-down temperature cycling: 2min 94^{o}C, ten cycles of (20s 94^{o}C, 30s 60^{o}C-to55^{o}C (dropping 0.5^{o}C per cycle), 45s 72^{o}C), 25 cycles of (20s 94^{o}C, 30s 55^{o}C, 45s 72^{o}C), 3min 72^{o}C.

Screening for *pik3cd*^{E525K} knock-in events used primers Ltest525 5'aaaactccaccgaattcttcaag3' and R1_525 5'atgagcaggagtttggggag3'. Tests for the established *pik3cd*^{E525K} allele used primers L2_525 5'tggattgaattgttgtagcacca3' and R1_525 5'atgagcaggagtttggggag3' followed by ApoI cleavage of the *pik3cd*^{E525K} sequence. Sequence analysis of *pik3cd*^{E525K} knock-in events was direct Sanger sequencing of PCR products from primers L2_525 with R1_525, or L3_525 5'gaattgttgtagcaccagaagc3' with R3_525 5'tgcacaaagagtaaacagcaca3' or L1_525 5'tggggctattgtgttgcatt3' with R2_525 5'tcacctgagccacatcctc3', using the PCR primers as sequencing primers.

Screening for *pik3cd*^{E1017K} knock-in events used primers Ltest_1017 5'actttaaggtcaaattcaacaaagc3' and R1_1017 5'cagtctgtgatcgagcgttg3'. Tests for the established *pik3cd*^{E1017K} allele used primers L1_1017 5'tgtcattggctgttcttgct3' and R1_1017, followed by ApoI cleavage of the *pik3cd*^{E1017K} sequence. The primer L2_1017 5'tcacaggactctttggcact3' was used with R1_1017 for genotyping degraded larvae following Staphylococcus infection. Sequence analysis of *pik3cd*^{E1017K} knock-in events was direct Sanger sequencing of PCR products from primers L1_1017 and R2_1017 5'gcaacatctccaaaagctgc3', using the PCR primers as sequencing primers.

ApoI digestion of PCR products used 0.5µl (5units) of ApoI (NEB) directly added to 20µl PCR reaction with 3hr 50^{o}C incubation.

Tail-fin injury assays

The *TgBAC(mpx:gfp)i114* 3dpf tail-fin injury inflammation time course assay followed (Renshaw et al. 2006). Transection was through the posterior tip of the notochord with a scalpel blade. Injured embryos were kept alone in 24 well plates. Neutrophils posterior to the circulatory loop were counted at successive time points using a Leica M165FC fluorescent stereo microscope.

For the 5dpf, Sudan black *TgBAC(mpx:gfp)i114* assay, transection was of the posterior tip of the tail-fin with a scalpel blade. At 2hpi, embryos were fixed for 1hr at room temperature in 4% PFA in PBS, rinsed three times with PBS, immersed 20min in Sudan Black B staining solution (Merck), 1hr in 70% ethanol with multiple changes, incrementally rehydrated into PBSTwE (PBS with 0.1% Tween-20, 1mM EDTA), mounted in a µ-slide (4-well glass bottom) (ibidi) in 1% low gelling temperature agarose in PBS and submerged in PBSTwE, then imaged in brightfield and a z-stack of fluorescent widefield with a Nikon Eclipse TE2000-U or Leica DMi8 inverted compound fluorescence microscope.

For the tail-fin regeneration assay, transection was through the posterior tip of the notochord with a scalpel blade at 3dpf. At 5dpf, embryos were mounted in 1% low gelling temperature agarose in E3 media, submerged in E3 and imaged with brightfield using a Nikon Eclipse TE2000-U or Leica DMi8 inverted compound microscope. The area of fin posterior to the notochord was manually traced and measured using Fiji.

For the 3dpf *TgBAC(il1b:EGFP)sh445* assay, transection was of the posterior tip of the tail-fin with a scalpel blade. At 3hpi, embryos were fixed for 90min at room temperature in 4% PFA in PBS, rinsed with PBSTwE, washed into TNT (0.1M Tris pH 7.5, 0.15M NaCl, 0.05% Tween-20), stained 30min in the dark without agitation in 1:50 Cyanine 5 Plus Amplification Reagent in Plus Amplification Dilutant (Perkin Elmer), washed into PBSTwE, mounted in a µ-slide (4-well glass bottom) (ibidi) in 1% low gelling temperature agarose in PBS and submerged in PBSTwE. A Nikon CSU W1 microscope with 25x silicon immersion lens collected spinning disk confocal z-stack images. For each embryo, a single neutrophil in the fin posterior to the notochord was analysed from maximal intensity projections of the z-

stacks. The Cy5 channel was used to segment the neutrophil using NIS Elements (Nikon) automatic region selector. The GFP channel average fluorescence intensity was measured within the neutrophil's selected region using NIS Elements.

Timelapse widefield video microscopy of *TgBAC(mpx:gfp)i114* neutrophil migration followed (Isles et al. 2021). 3dpf embryos were mounted in 1% low gelling temperature agarose in E3 media, submerged in E3 and then a 30G syringe needle was used to cut a small notch on the ventral side of the tail-fin immediately before capturing a 6hr timelapse series using a Nikon Eclipse TE2000-U inverted compound fluorescence microscope. Semi-automated tracking of fluorescent neutrophils used NIS Elements (version 4.3) with an additional NIS elements tracking module. Maximal intensity projections were used to generate a binary layer that was smoothed, cleaned and separated to enable tracking. Neutrophils were only tracked if they reached the wound and those neutrophils were tracked until they reached the wound.

Whole body neutrophil and macrophage counts

For lightsheet microscopy, *TgBAC(mpx:gfp)i114* or *Tg(mpeg1.1:NLS-clover)sh616* embryos were embedded in groups of three in 1% low gelling temperature agarose in E3 in a mounting capillary, imaged with a ZEISS Light Sheet Z.1, and then individually collected for PCR genotyping. Each embryo was imaged with z-stacks through the head and trunk from each side and a z-stack through the tail. Fluorescent cells were manually counted from z-stacks using the Fiji point tool. Manual inspection ensured cells were not double counted between the views.

For spinning disk microscopy of CAL-101 treated and control *TgBAC(mpx:gfp)i114* embryos, alternate groups of 24 treated or control embryos were mounted in the wells of a µ-slide (4-well glass bottom) (ibidi) in 1% low gelling temperature agarose in E3 and submerged in E3. Brightfield and a z-stack of spinning disk confocal images (350µm range, 5µm increments) used a Nikon CSU W1 microscope with 10x lens. Each embryo was imaged at three axial positions set automatically to create a merged tiled image. The set of embryos were imaged together as an automated multipoint series within a 2hr time window.

Fluorescent cells were manually counted from a maximal intensity projection of the fluorescent channel using the Fiji point tool. Every embryo was counted at the same brightness-contrast setting.

Whole kidney marrow flow cytometry

Whole kidney marrow (WKM) from adult *TgBAC(mpx:gfp)i114* zebrafish was dissected following (Gerlach et al. 2011) and collected into 200µl live sorting buffer (80% Leibovitz's L-15 media (ThermoFisher), 20% foetal bovine serum, 5mM EDTA) on ice. Immediately before flow cytometry, WKM was macerated by pipetting, passed through a 40µm cell strainer, rinsed through by addition of 400µl PBS, then 5µl 1mM TO-PRO-3 (ThermoFisher) stain added. From each sample, 10^5 cells were analysed with a BD FACSMelody cell sorter. Sorting was based on forward scatter and side scatter to identify leukocyte and precursor single cells following (Traver et al. 2003), TO-PRO-3 fluorescence to exclude non-viable cells and GFP fluorescence to identify neutrophils. Analysis was performed using BD FACSChorus software (BD Biosciences).

Staphylococcus aureus infection

Infection assays followed (Prajsnar et al. 2008). Embryos mounted in 3% methylcellulose (Merk) in E3 were injected, at 30hpf, with 1500cfu *Staphylococcus aureus* (strain SH1000) in 1nl 2% Polyvinylpyrrolidone (Merk) in PBS with phenol red (Merk), into the duct of cuvier. After soaking in E3 to release the embryos, undamaged embryos were transferred to individual wells of 96 well plates. They were inspected each morning and evening using a stereo microscope. Any without a heartbeat or with extensive necrosis were collected and stored at -20^{o}C until genotyping.

Statistics and image analysis

Graphpad Prism9 was used for statistics and charts. Fiji was used for image analysis (Schindelin et al. 2012). Figures were prepared using Fiji and Adobe Photoshop.

Acknowledgements

We gratefully acknowledge David Drew for laboratory management, Catherine Loynes and Naznin Choudhury for expert advice, Kathryn Adamson and Phil Elks for helpful discussions and the University of Sheffield Biological Services Aquarium, Flow Cytometry Core Service and Wolfson Light Microscope Facility. Funding for the project was from the Medical Research Council MR/M012328/2 (A.M.C.) and antimicrobial resistance cross-council funding from the Medical Research Council to The Universities of Sheffield, Birmingham, Edinburgh and Newcastle Led partnership to Develop Host Defence Therapeutics (SHIELD) consortium "Optimising Innate Host Defence to Combat Antimicrobial Resistance" MRNO2995X/1 (S.A.R and A.M.C).

Author Contributions

Conceptualisation: K.V., A.M.C., S.A.R.; Methodology: S.E., S.A.R., N.M.H., T.K.P., H.A.R., A.M.C.; Validation: S.E.; Formal analysis: S.E.; Investigation: S.E., H.A.R.; Resources: S.A.R., A.M.C.; Data curation; S.E.; Writing-original draft preparation: S.E.; Writing-review and editing: S.E., S.A.R., N.M.H., A.M.C., K.V., T.K.P., H.A.R.; Visualisation: S.E.; Supervision: S.A.R., N.M.H., A.M.C.; Project administration: S.A.R., A.M.C.; Funding acquisition: A.M.C.

Competing interests

The authors declare no competing or financial interests.

References

Angulo, I., O. Vadas, F. Garcon, E. Banham-Hall, V. Plagnol, T. R. Leahy, H. Baxendale, T. Coulter, J. Curtis, C. Wu, et al. (2013). "Phosphoinositide 3-kinase delta gene mutation predisposes to respiratory infection and airway damage." Science **342**(6160): 866-871.

Athanasiadis, E. I., J. G. Botthof, H. Andres, L. Ferreira, P. Lio and A. Cvejic (2017). "Single-cell RNA-sequencing uncovers transcriptional states and fate decisions in haematopoiesis." Nat Commun **8**(1): 2045.

Avery, D. T., A. Kane, T. Nguyen, A. Lau, A. Nguyen, H. Lenthall, K. Payne, W. Shi, H. Brigden, E. French, et al. (2018). "Germline-activating mutations in PIK3CD compromise B cell development and function." J Exp Med **215**(8): 2073-2095.

Bernut, A., C. Dupont, N. V. Ogryzko, A. Neyret, J. L. Herrmann, R. A. Floto, S. A. Renshaw and L. Kremer (2019). "CFTR Protects against Mycobacterium abscessus Infection by Fine-Tuning Host Oxidative Defenses." Cell Rep **26**(7): 1828-1840 e1824.

Bernut, A., C. A. Loynes, R. A. Floto and S. A. Renshaw (2020). "Deletion of cftr Leads to an Excessive Neutrophilic Response and Defective Tissue Repair in a Zebrafish Model of Sterile Inflammation." Front Immunol **11**: 1733.

Bin Moon, S., J. M. Lee, J. G. Kang, N. E. Lee, D. I. Ha, D. Y. Kim, S. H. Kim, K. Yoo, D. Kim, J. H. Ko, et al. (2018). "Highly efficient genome editing by CRISPR-Cpf1 using CRISPR RNA with a uridinylate-rich 3'-overhang." Nat Commun **9**(1): 3651.

Boel, A., H. De Saffel, W. Steyaert, B. Callewaert, A. De Paepe, P. J. Coucke and A. Willaert (2018). "CRISPR/Cas9-mediated homology-directed repair by ssODNs in zebrafish induces complex mutational patterns resulting from genomic integration of repair-template fragments." Dis Model Mech **11**(10).

Bonkhofer, F., R. Rispoli, P. Pinheiro, M. Krecsmarik, J. Schneider-Swales, I. H. C. Tsang, M. de Bruijn, R. Monteiro, T. Peterkin and R. Patient (2019). "Blood stem cell-forming haemogenic endothelium in zebrafish derives from arterial endothelium." Nat Commun **10**(1): 3577.

Brodsky, N. N. and C. L. Lucas (2021). "Infections in activated PI3K delta syndrome (APDS)." Curr Opin Immunol **72**: 146-157.

Browning, M. J., A. Chandra, V. Carbonaro, K. Okkenhaug and J. Barwell (2015). "Cowden's syndrome with immunodeficiency." J Med Genet **52**(12): 856-859.

Burke, J. E. and R. L. Williams (2015). "Synergy in activating class I PI3Ks." Trends Biochem Sci **40**(2): 88-100.

Chiriaco, M., I. Brigida, P. Ariganello, S. Di Cesare, G. Di Matteo, F. Taus, D. Cittaro, D. Lazarevic, A. Scarselli, V. Santilli, et al. (2017). "The case of an APDS patient: Defects in maturation and function and decreased in vitro anti-mycobacterial activity in the myeloid compartment." Clin Immunol **178**: 20-28.

Choorapoikayil, S., R. Kers, P. Herbomel, K. Kissa and J. den Hertog (2014). "Pivotal role of Pten in the balance between proliferation and differentiation of hematopoietic stem cells in zebrafish." Blood **123**(2): 184-190.

Condliffe, A. M. and A. Chandra (2018). "Respiratory Manifestations of the Activated Phosphoinositide 3-Kinase Delta Syndrome." Front Immunol **9**: 338.
Condliffe, A. M., K. Davidson, K. E. Anderson, C. D. Ellson, T. Crabbe, K. Okkenhaug, B. Vanhaesebroeck, M. Turner, L. Webb, M. P. Wymann, et al. (2005). "Sequential activation of class IB and class IA PI3K is important for the primed respiratory burst of human but not murine neutrophils." Blood **106**(4): 1432-1440.
Cornillet-Lefebvre, P., W. Cuccuini, V. Bardet, J. Tamburini, L. Gillot, N. Ifrah, P. Nguyen, F. Dreyfus, P. Mayeux, C. Lacombe, et al. (2006). "Constitutive phosphoinositide 3-kinase activation in acute myeloid leukemia is not due to p110delta mutations." Leukemia **20**(2): 374-376.
Darici, S., H. Alkhaldi, G. Horne, H. G. Jorgensen, S. Marmiroli and X. Huang (2020). "Targeting PI3K/Akt/mTOR in AML: Rationale and Clinical Evidence." J Clin Med **9**(9).
de Weerdt, I., S. M. Koopmans, A. P. Kater and M. van Gelder (2017). "Incidence and management of toxicity associated with ibrutinib and idelalisib: a practical approach." Haematologica **102**(10): 1629-1639.
Desmet, F. O., D. Hamroun, M. Lalande, G. Collod-Beroud, M. Claustres and C. Beroud (2009). "Human Splicing Finder: an online bioinformatics tool to predict splicing signals." Nucleic Acids Res **37**(9): e67.
Dornan, G. L., B. D. Siempelkamp, M. L. Jenkins, O. Vadas, C. L. Lucas and J. E. Burke (2017). "Conformational disruption of PI3Kdelta regulation by immunodeficiency mutations in PIK3CD and PIK3R1." Proc Natl Acad Sci U S A **114**(8): 1982-1987.
Dovi, J. V., L. K. He and L. A. DiPietro (2003). "Accelerated wound closure in neutrophil-depleted mice." J Leukoc Biol **73**(4): 448-455.
Farnsworth, D. R., L. M. Saunders and A. C. Miller (2020). "A single-cell transcriptome atlas for zebrafish development." Dev Biol **459**(2): 100-108.
Fernandez, J. P., C. E. Vejnar, A. J. Giraldez, R. Rouet and M. A. Moreno-Mateos (2018). "Optimized CRISPR-Cpf1 system for genome editing in zebrafish." Methods **150**: 11-18.
Gerlach, G. F., L. N. Schrader and R. A. Wingert (2011). "Dissection of the adult zebrafish kidney." J Vis Exp(54).
Hall, C. J., M. V. Flores, S. H. Oehlers, L. E. Sanderson, E. Y. Lam, K. E. Crosier and P. S. Crosier (2012). "Infection-responsive expansion of the hematopoietic stem and progenitor cell compartment in zebrafish is dependent upon inducible nitric oxide." Cell Stem Cell **10**(2): 198-209.

Hannigan, M., L. Zhan, Z. Li, Y. Ai, D. Wu and C. K. Huang (2002). "Neutrophils lacking phosphoinositide 3-kinase gamma show loss of directionality during N-formyl-Met-Leu-Phe-induced chemotaxis." Proc Natl Acad Sci U S A **99**(6): 3603-3608.

Hirsch, E., V. L. Katanaev, C. Garlanda, O. Azzolino, L. Pirola, L. Silengo, S. Sozzani, A. Mantovani, F. Altruda and M. P. Wymann (2000). "Central role for G protein-coupled phosphoinositide 3-kinase gamma in inflammation." Science **287**(5455): 1049-1053.

Isles, H. M., C. A. Loynes, S. Alasmari, F. C. Kon, K. M. Henry, A. Kadochnikova, J. Hales, C. F. Muir, M. C. Keightley, V. Kadirkamanathan, et al. (2021). "Pioneer neutrophils release chromatin within in vivo swarms." Elife **10**.

Jou, S. T., Y. H. Chien, Y. H. Yang, T. C. Wang, S. D. Shyur, C. C. Chou, M. L. Chang, D. T. Lin, K. H. Lin and B. L. Chiang (2006). "Identification of variations in the human phosphoinositide 3-kinase p110delta gene in children with primary B-cell immunodeficiency of unknown aetiology." Int J Immunogenet **33**(5): 361-369.

Kharas, M. G., R. Okabe, J. J. Ganis, M. Gozo, T. Khandan, M. Paktinat, D. G. Gilliland and K. Gritsman (2010). "Constitutively active AKT depletes hematopoietic stem cells and induces leukemia in mice." Blood **115**(7): 1406-1415.

Kim, H. K., S. Min, M. Song, S. Jung, J. W. Choi, Y. Kim, S. Lee, S. Yoon and H. H. Kim (2018). "Deep learning improves prediction of CRISPR-Cpf1 guide RNA activity." Nat Biotechnol **36**(3): 239-241.

Kwak, H. J., P. Liu, B. Bajrami, Y. Xu, S. Y. Park, C. Nombela-Arrieta, S. Mondal, Y. Sun, H. Zhu, L. Chai, et al. (2015). "Myeloid cell-derived reactive oxygen species externally regulate the proliferation of myeloid progenitors in emergency granulopoiesis." Immunity **42**(1): 159-171.

Labun, K., T. G. Montague, J. A. Gagnon, S. B. Thyme and E. Valen (2016). "CHOPCHOP v2: a web tool for the next generation of CRISPR genome engineering." Nucleic Acids Res **44**(W1): W272-276.

Lannutti, B. J., S. A. Meadows, S. E. Herman, A. Kashishian, B. Steiner, A. J. Johnson, J. C. Byrd, J. W. Tyner, M. M. Loriaux, M. Deininger, et al. (2011). "CAL-101, a p110delta selective phosphatidylinositol-3-kinase inhibitor for the treatment of B-cell malignancies, inhibits PI3K signaling and cellular viability." Blood **117**(2): 591-594.

Li, L., B. Yan, Y. Q. Shi, W. Q. Zhang and Z. L. Wen (2012). "Live imaging reveals differing roles of macrophages and neutrophils during zebrafish tail fin regeneration." J Biol Chem **287**(30): 25353-25360.

Li, Z., H. Jiang, W. Xie, Z. Zhang, A. V. Smrcka and D. Wu (2000). "Roles of PLC-beta2 and -beta3 and PI3Kgamma in chemoattractant-mediated signal transduction." Science **287**(5455): 1046-1049.

Lieschke, G. J., A. C. Oates, M. O. Crowhurst, A. C. Ward and J. E. Layton (2001). "Morphologic and functional characterization of granulocytes and macrophages in embryonic and adult zebrafish." Blood **98**(10): 3087-3096.

Lister, J. A., C. P. Robertson, T. Lepage, S. L. Johnson and D. W. Raible (1999). "nacre encodes a zebrafish microphthalmia-related protein that regulates neural-crest-derived pigment cell fate." Development **126**(17): 3757-3767.

Liu, L., K. D. Puri, J. M. Penninger and P. Kubes (2007). "Leukocyte PI3Kgamma and PI3Kdelta have temporally distinct roles for leukocyte recruitment in vivo." Blood **110**(4): 1191-1198.

Lu, M., W. Gu, Y. Sheng, J. Wang and X. Xu (2021). "Case Report: Activating PIK3CD Mutation in Patients Presenting With Granulomatosis With Polyangiitis." Front Immunol **12**: 670312.

Lucas, C. L., A. Chandra, S. Nejentsev, A. M. Condliffe and K. Okkenhaug (2016). "PI3Kdelta and primary immunodeficiencies." Nat Rev Immunol **16**(11): 702-714.

Lucas, C. L., H. S. Kuehn, F. Zhao, J. E. Niemela, E. K. Deenick, U. Palendira, D. T. Avery, L. Moens, J. L. Cannons, M. Biancalana, et al. (2014). "Dominant-activating germline mutations in the gene encoding the PI(3)K catalytic subunit p110delta result in T cell senescence and human immunodeficiency." Nat Immunol **15**(1): 88-97.

Michalovich, D. and S. Nejentsev (2018). "Activated PI3 Kinase Delta Syndrome: From Genetics to Therapy." Front Immunol **9**: 369.

Mistry, J. J., C. R. Marlein, J. A. Moore, C. Hellmich, E. E. Wojtowicz, J. G. W. Smith, I. Macaulay, Y. Sun, A. Morfakis, A. Patterson, et al. (2019). "ROS-mediated PI3K activation drives mitochondrial transfer from stromal cells to hematopoietic stem cells in response to infection." Proc Natl Acad Sci U S A **116**(49): 24610-24619.

Moreno-Mateos, M. A., J. P. Fernandez, R. Rouet, C. E. Vejnar, M. A. Lane, E. Mis, M. K. Khokha, J. A. Doudna and A. J. Giraldez (2017). "CRISPR-Cpf1 mediates efficient homology-directed repair and temperature-controlled genome editing." Nat Commun **8**(1): 2024.

Nishio, M., K. Watanabe, J. Sasaki, C. Taya, S. Takasuga, R. Iizuka, T. Balla, M. Yamazaki, H. Watanabe, R. Itoh, et al. (2007). "Control of cell polarity and motility by the PtdIns(3,4,5)P3 phosphatase SHIP1." Nat Cell Biol **9**(1): 36-44.

Nunes-Santos, C. J., G. Uzel and S. D. Rosenzweig (2019). "PI3K pathway defects leading to immunodeficiency and immune dysregulation." J Allergy Clin Immunol **143**(5): 1676-1687.
Ogryzko, N. V., A. Lewis, H. L. Wilson, A. H. Meijer, S. A. Renshaw and P. M. Elks (2019). "Hif-1alpha-Induced Expression of Il-1beta Protects against Mycobacterial Infection in Zebrafish." J Immunol **202**(2): 494-502.
Okkenhaug, K., A. Bilancio, G. Farjot, H. Priddle, S. Sancho, E. Peskett, W. Pearce, S. E. Meek, A. Salpekar, M. D. Waterfield, et al. (2002). "Impaired B and T cell antigen receptor signaling in p110delta PI 3-kinase mutant mice." Science **297**(5583): 1031-1034.
Park, H. M., H. Liu, J. Wu, A. Chong, V. Mackley, C. Fellmann, A. Rao, F. Jiang, H. Chu, N. Murthy, et al. (2018). "Extension of the crRNA enhances Cpf1 gene editing in vitro and in vivo." Nat Commun **9**(1): 3313.
Prajsnar, T. K., V. T. Cunliffe, S. J. Foster and S. A. Renshaw (2008). "A novel vertebrate model of Staphylococcus aureus infection reveals phagocyte-dependent resistance of zebrafish to non-host specialized pathogens." Cell Microbiol **10**(11): 2312-2325.
Prajsnar, T. K., R. Hamilton, J. Garcia-Lara, G. McVicker, A. Williams, M. Boots, S. J. Foster and S. A. Renshaw (2012). "A privileged intraphagocyte niche is responsible for disseminated infection of Staphylococcus aureus in a zebrafish model." Cell Microbiol **14**(10): 1600-1619.
Prykhozhij, S. V. and J. N. Berman (2018). "Zebrafish knock-ins swim into the mainstream." Dis Model Mech **11**(10).
Prykhozhij, S. V., C. Fuller, S. L. Steele, C. J. Veinotte, B. Razaghi, J. M. Robitaille, C. R. McMaster, A. Shlien, D. Malkin and J. N. Berman (2018). "Optimized knock-in of point mutations in zebrafish using CRISPR/Cas9." Nucleic Acids Res **46**(17): e102.
Rao, V. K., S. Webster, V. Dalm, A. Sediva, P. M. van Hagen, S. Holland, S. D. Rosenzweig, A. D. Christ, B. Sloth, M. Cabanski, et al. (2017). "Effective "activated PI3Kdelta syndrome"-targeted therapy with the PI3Kdelta inhibitor leniolisib." Blood **130**(21): 2307-2316.
Reese, M. G., F. H. Eeckman, D. Kulp and D. Haussler (1997). "Improved splice site detection in Genie." J Comput Biol **4**(3): 311-323.
Renshaw, S. A., C. A. Loynes, D. M. Trushell, S. Elworthy, P. W. Ingham and M. K. Whyte (2006). "A transgenic zebrafish model of neutrophilic inflammation." Blood **108**(13): 3976-3978.

Sadhu, C., B. Masinovsky, K. Dick, C. G. Sowell and D. E. Staunton (2003). "Essential role of phosphoinositide 3-kinase delta in neutrophil directional movement." J Immunol **170**(5): 2647-2654.

Sapey, E., H. Greenwood, G. Walton, E. Mann, A. Love, N. Aaronson, R. H. Insall, R. A. Stockley and J. M. Lord (2014). "Phosphoinositide 3-kinase inhibition restores neutrophil accuracy in the elderly: toward targeted treatments for immunosenescence." Blood **123**(2): 239-248.

Sapey, E., J. A. Stockley, H. Greenwood, A. Ahmad, D. Bayley, J. M. Lord, R. H. Insall and R. A. Stockley (2011). "Behavioral and structural differences in migrating peripheral neutrophils from patients with chronic obstructive pulmonary disease." Am J Respir Crit Care Med **183**(9): 1176-1186.

Sasaki, T., J. Irie-Sasaki, R. G. Jones, A. J. Oliveira-dos-Santos, W. L. Stanford, B. Bolon, A. Wakeham, A. Itie, D. Bouchard, I. Kozieradzki, et al. (2000). "Function of PI3Kgamma in thymocyte development, T cell activation, and neutrophil migration." Science **287**(5455): 1040-1046.

Schindelin, J., I. Arganda-Carreras, E. Frise, V. Kaynig, M. Longair, T. Pietzsch, S. Preibisch, C. Rueden, S. Saalfeld, B. Schmid, et al. (2012). "Fiji: an open-source platform for biological-image analysis." Nat Methods **9**(7): 676-682.

Singh, A., V. Joshi, A. K. Jindal, B. Mathew and A. Rawat (2020). "An updated review on activated PI3 kinase delta syndrome (APDS)." Genes Dis **7**(1): 67-74.

Smith, P. J., C. Zhang, J. Wang, S. L. Chew, M. Q. Zhang and A. R. Krainer (2006). "An increased specificity score matrix for the prediction of SF2/ASF-specific exonic splicing enhancers." Hum Mol Genet **15**(16): 2490-2508.

Stark, A. K., A. Chandra, K. Chakraborty, R. Alam, V. Carbonaro, J. Clark, S. Sriskantharajah, G. Bradley, A. G. Richter, E. Banham-Hall, et al. (2018). "PI3Kdelta hyper-activation promotes development of B cells that exacerbate Streptococcus pneumoniae infection in an antibody-independent manner." Nat Commun **9**(1): 3174.

Tang, Q., S. Iyer, R. Lobbardi, J. C. Moore, H. Chen, C. Lareau, C. Hebert, M. L. Shaw, C. Neftel, M. L. Suva, et al. (2017). "Dissecting hematopoietic and renal cell heterogeneity in adult zebrafish at single-cell resolution using RNA sequencing." J Exp Med **214**(10): 2875-2887.

Traver, D., B. H. Paw, K. D. Poss, W. T. Penberthy, S. Lin and L. I. Zon (2003). "Transplantation and in vivo imaging of multilineage engraftment in zebrafish bloodless mutants." Nat Immunol **4**(12): 1238-1246.

Tsarouchas, T. M., D. Wehner, L. Cavone, T. Munir, M. Keatinge, M. Lambertus, A. Underhill, T. Barrett, E. Kassapis, N. Ogryzko, et al. (2018). "Dynamic control of proinflammatory cytokines Il-1beta and Tnf-alpha by macrophages in zebrafish spinal cord regeneration." Nat Commun **9**(1): 4670.

Untergasser, A., I. Cutcutache, T. Koressaar, J. Ye, B. C. Faircloth, M. Remm and S. G. Rozen (2012). "Primer3--new capabilities and interfaces." Nucleic Acids Res **40**(15): e115.

Wray-Dutra, M. N., F. Al Qureshah, G. Metzler, M. Oukka, R. G. James and D. J. Rawlings (2018). "Activated PIK3CD drives innate B cell expansion yet limits B cell-intrinsic immune responses." J Exp Med **215**(10): 2485-2496.

Xie, X., M. Liu, Y. Zhang, B. Wang, C. Zhu, C. Wang, Q. Li, Y. Huo, J. Guo, C. Xu, et al. (2021). "Single-cell transcriptomic landscape of human blood cells." Natl Sci Rev **8**(3): nwaa180.

Xu, H., T. Xiao, C. H. Chen, W. Li, C. A. Meyer, Q. Wu, D. Wu, L. Cong, F. Zhang, J. S. Liu, et al. (2015). "Sequence determinants of improved CRISPR sgRNA design." Genome Res **25**(8): 1147-1157.

Yilmaz, O. H., R. Valdez, B. K. Theisen, W. Guo, D. O. Ferguson, H. Wu and S. J. Morrison (2006). "Pten dependence distinguishes haematopoietic stem cells from leukaemia-initiating cells." Nature **441**(7092): 475-482.

Yoo, S. K., Q. Deng, P. J. Cavnar, Y. I. Wu, K. M. Hahn and A. Huttenlocher (2010). "Differential regulation of protrusion and polarity by PI3K during neutrophil motility in live zebrafish." Dev Cell **18**(2): 226-236.

Zhang, J., J. C. Grindley, T. Yin, S. Jayasinghe, X. C. He, J. T. Ross, J. S. Haug, D. Rupp, K. S. Porter-Westpfahl, L. M. Wiedemann, et al. (2006). "PTEN maintains haematopoietic stem cells and acts in lineage choice and leukaemia prevention." Nature **441**(7092): 518-522.

Figures

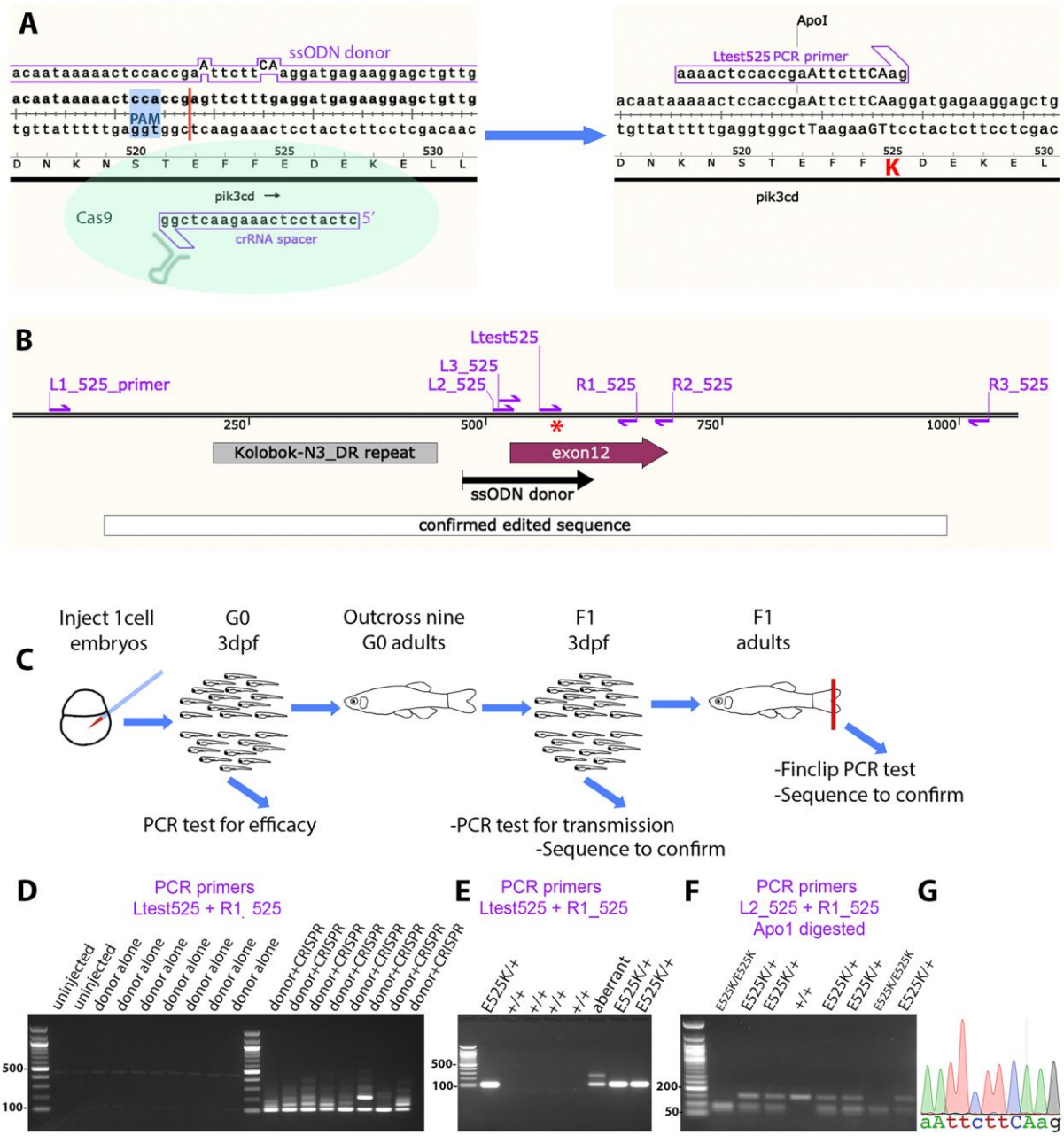

Fig. 1. Homology directed CRISPR-Cas9 knock-in of a *pik3cd*^{E525K} allele. (**A**) Diagram illustrating the knock-in process. The CRISPR-Cas9 cleavage and knock-in is illustrated on the left and the resulting *pik3cd*^{E525K} allele on the right. On the left, the ssODN donor sequence and crRNA spacer sequence are positioned alongside the *pik3cd* DNA sequence and translated amino acid sequence, with the CRISPR-Cas9 PAM highlighted in blue and the

cleavage site shown as a red line. On the right, mutated DNA bases are shown in uppercase, the E525K coding change is highlighted in red and the introduced ApoI cleavage site is indicated. The Ltest525 PCR Primer is specific for the knock-in allele. (**B**) Map of the zebrafish *pik3cd*^{E525K} locus. PCR primers are shown as magenta arrows; the mutation site is marked with red asterisks; and positions are shown for: the ssODN donor used for knock-in, the region confirmed by sequencing after knock-in, *pik3cd* exon12, a DNA repeat incompatible with PCR primer location. (**C**) Diagram illustrating the workflow for establishing the line with the *pik3cd*^{E525K} allele. (**D**) Agarose electrophoresis gel with knock-in-specific test PCRs from 3dpf G0 embryos. All the embryos previously injected with CRISPR-Cas9 and ssODN donor produced the expected 103bp amplicon and also lower electrophoretic mobility products. PCRs from uninjected embryos, or embryos injected with CRISPR-Cas9 alone, did not amplify. DNA size marker is a 100bp ladder. (**E**) Agarose electrophoresis gel with knock-in-specific test PCRs from 3dpf F1 embryos from an outcross of a G0 adult that had been injected with CRISPR-Cas9 and ssODN donor when an embryo. PCRs from embryos with the *pik3cd*^{E525K} allele produce a 103bp amplicon. A lower mobility band indicates a putative aberrant knock-in event. DNA size marker is 100bp ladder. (**F**) Agarose electrophoresis gel with Apo1 digested PCR amplicons from F2 embryos from a *pik3cd*$^{E525K/+}$ in-cross. The *pik3cd*^{E52K5} allele introduces an Apo1 site allowing *pik3cd*$^{E525K/E525K}$, *pik3cd*$^{E525K/+}$ and *pik3cd*$^{+/+}$ genotypes to be distinguished. DNA size marker is 50bp ladder. (**G**) Sanger sequencing trace from a PCR amplicon across the knock-in locus of a *pik3cd*$^{E525K/E525K}$ F2 adult. The mutated DNA bases are shown in uppercase as in (A).

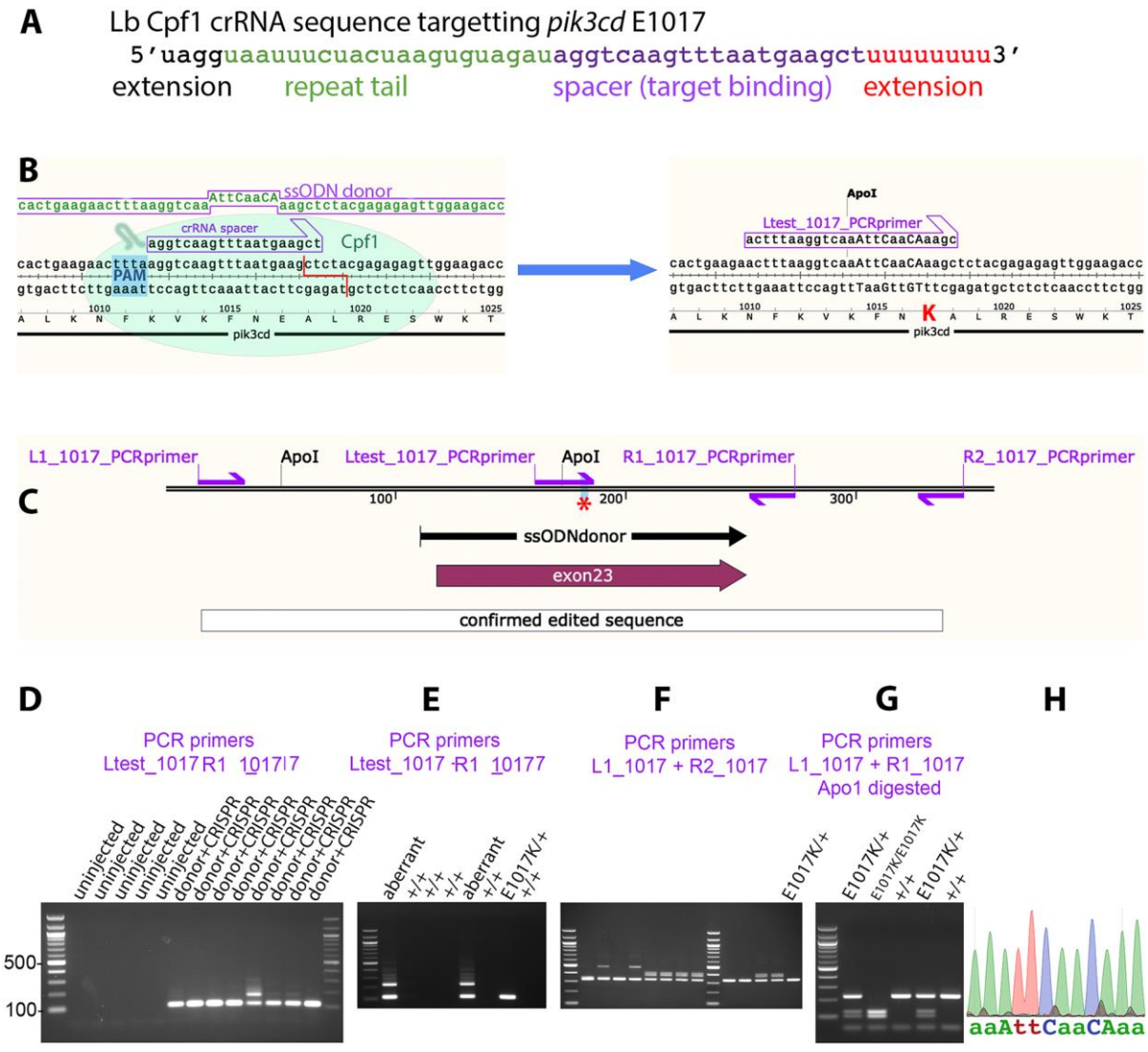

Fig. 2. Homology directed CRISPR-LbCpf1 knock-in of a *pik3cd*^{E1017K} allele. (**A**) Sequence of crRNA oligonucleotide, showing 5' and 3' extensions beyond the minimal sequence of repeat tail and target binding spacer. **(B)** Diagram illustrating the knock-in process. The CRISPR-LbCpf1 cleavage and knock-in is illustrated on the left and the resulting *pik3cd*^{E1017K} allele on the right. On the left, the ssODN donor sequence and crRNA spacer sequence are positioned alongside the *pik3cd* DNA sequence and translated amino acid sequence, with the CRISPR-LbCpf1 PAM highlighted in blue and the cleavage site shown as a red line. On the right, mutated DNA bases are shown in uppercase, the E1017K coding change is highlighted in red and the introduced ApoI cleavage site is indicated. The Ltest_1017 PCR Primer is specific for the knock-in allele. (**C**) Map of the zebrafish *pik3cd*^{E1017K} locus. PCR primers are shown as magenta arrows; the mutation site is marked with red asterisks; and positions are shown for: the ssODN donor used for knock-in, the

region confirmed by sequencing after knock-in, and *pik3cd* exon23. (**D**) Agarose electrophoresis gel with knock-in-specific test PCRs from 3dpf G0 embryos. All the embryos previously injected with CRISPR-LbCpf1 and ssODN donor produced the expected 113bp amplicon and sometimes also lower electrophoretic mobility products. PCRs from uninjected embryos did not amplify. DNA size marker is 100bp ladder. (**E**) Agarose electrophoresis gel with knock-in-specific test PCRs from 3dpf F1 embryos from an outcross of a G0 adult that had been injected with CRISPR-LbCpf1 and ssODN donor when an embryo. A *pik3cd*$^{E1017K/+}$ embryo produced the 113bp amplicon whilst other embryos produced lower mobility amplicons indicating aberrant knock-in events. DNA size marker is 100bp ladder. (**F**) Agarose electrophoresis gel with PCRs spanning the knock-in locus to further test embryos that had given the expected 113bp amplicon with test PCRs as in (E). The *pik3cd*$^{E1017K/+}$ embryo indicated in (E) gave the expected 332bp amplicon but some other embryos produced lower mobility amplicons indicating aberrant knock-in events despite having given the expected 113bp amplicon with test PCRs as in (E). (**G**) Agarose electrophoresis gel with Apo1 digested PCR amplicons from F2 adults from a *pik3cd*$^{E1017K/+}$ in-cross. The *pik3cd*^{E1017K} allele introduces an Apo1 site allowing *pik3cd*$^{E1017K/E1017K}$, *pik3cd*$^{E1017K/+}$ and *pik3cd*$^{+/+}$ genotypes to be distinguished. DNA size marker is 100bp ladder. (**H**) Sanger sequencing trace from a PCR amplicon across the knock-in locus of a *pik3cd*$^{E1017K/E1017K}$ F2 adult. The mutated DNA bases are shown in uppercase as in (B).

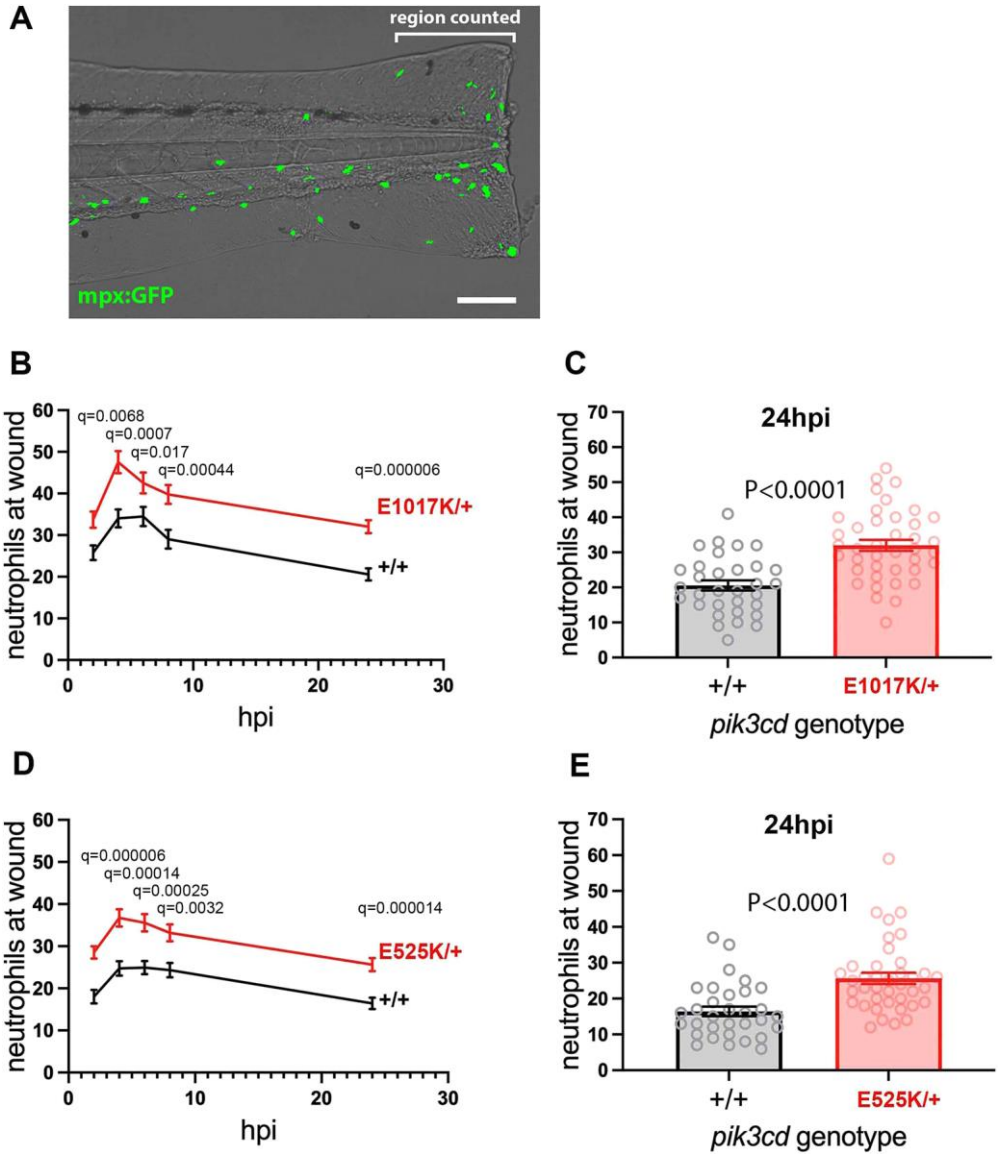

Fig. 3. Neutrophilic inflammation following tail-fin injury of *pik3cd*$^{E1017K/+}$ embryos and *pik3cd*$^{E525K/+}$ embryos. (A) Composite brightfield and maximal projection of widefield fluorescent (shown in green) micrograph stack illustrating the *TgBAC(mpx:gfp)i114* 3dpf embryo tail-fin injury used to analyse inflammation response. Transection is through the tip of the notochord and GFP marked neutrophils counted proximal to the circulatory loop. Scale bar 100µm. (**B**) Chart of the tail-fin injury inflammation time course for 72, 3dpf embryos from a *pik3cd*$^{E1017K/+}$ outcross. Successive neutrophil counts at the injury site are shown as the mean±SEM for embryos subsequently genotyped as *pik3cd*$^{E1017K/+}$ (red) or *pik3cd*$^{+/+}$ (black). Multiple Mann-Whitney tests. (**C**) Chart with the same data as in (B) but showing the neutrophil counts for the individual embryos at the 24hpi end point of the analysis. Mann-Whitney test. Data shown are from one experiment. A repeat experiment with 71 embryos

showed the same effect (at p<0.0001 at 24hpi) as did a 36 embryo, 4hpi time point, pilot experiment (at p=0.001). (**D**) Chart of the tail-fin injury inflammation time course for 71, 3dpf embryos from a *pik3cd*$^{E525K/+}$ outcross. Successive neutrophil counts at the injury site are shown as the mean±SEM for embryos subsequently genotyped as *pik3cd*$^{E525K/+}$ (red) or *pik3cd*$^{+/+}$ (black). Multiple Mann-Whitney tests. (**E**) Chart with the same data as in (D) but showing the neutrophil counts for the individual embryos at the 24hpi end point of the analysis. Mann-Whitney test. Data shown are from one experiment. A repeat experiment with 96 embryos showed the same effect (at p=0.0004 at 24hpi)

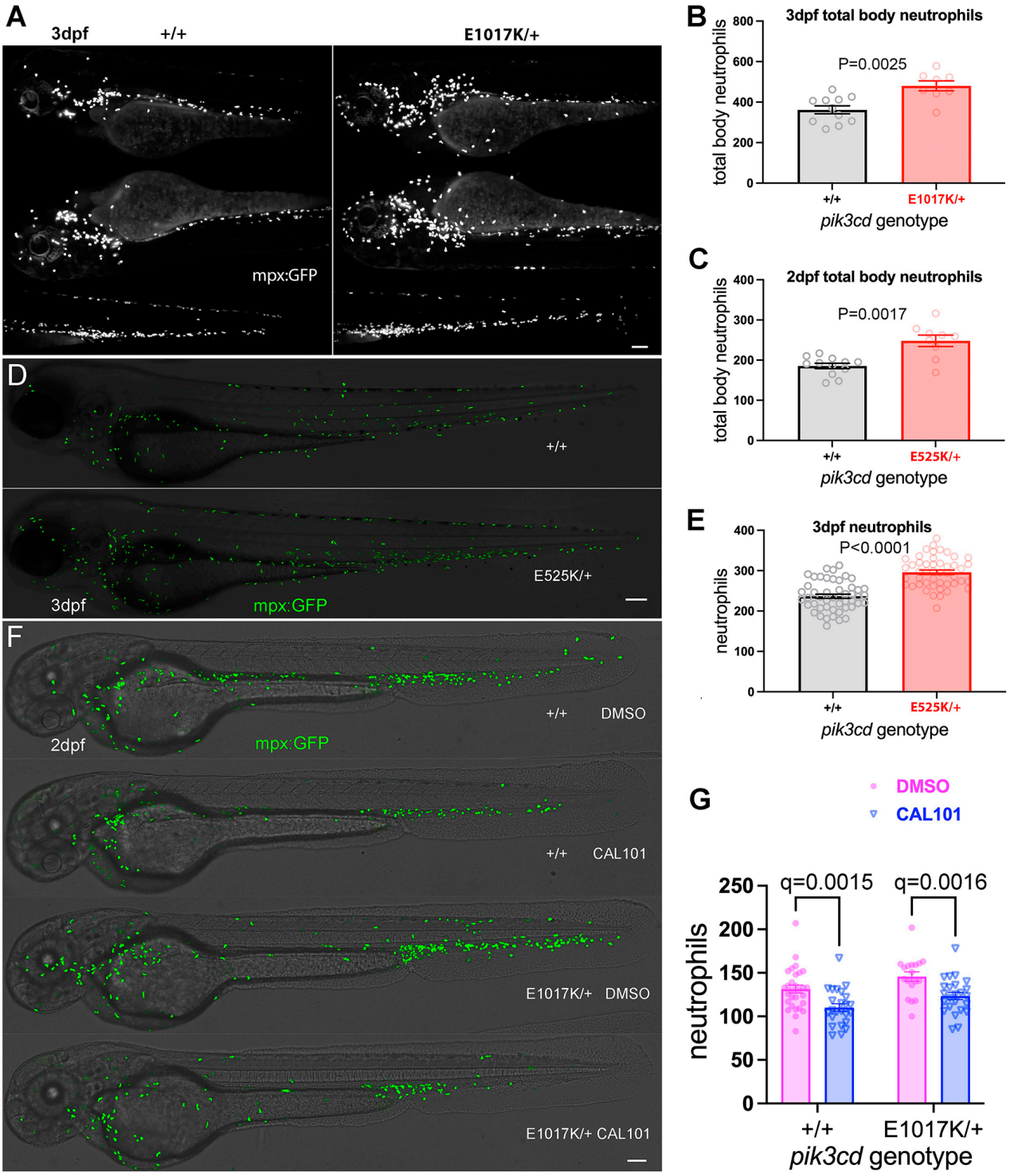

Fig. 4. Effect on total body neutrophils from *pik3cd*$^{E1017K/+}$ and *pik3cd*$^{E525K/+}$ genotype and the PI3Kδ inhibitor CAL-101. (**A**) Light sheet microscopy used to count total body *TgBAC(mpx:gfp)i114* neutrophils of *pik3cd*$^{E1017K/+}$ and *pik3cd*$^{+/+}$ 3dpf, sibling embryos. Upper panels show maximal intensity projections for the three views used for each embryo. Scale bar 100μm. (**B**) Chart of total body neutrophils counted from light sheet microscopy views as in (A) for 19 sibling 2dpf *pik3cd*$^{E1017K/+}$ and *pik3cd*$^{+/+}$ embryos. Bars show the

mean±SEM, Mann-Whitney test. Single experiment. (**C**) Chart of total body neutrophils counted from light sheet microscopy views as in (A) but for 21 *pik3cd*$^{E525K/+}$ and *pik3cd*$^{+/+}$ 2dpf sibling embryos. Bars show the mean±SEM, Mann-Whitney test. Single experiment. (**D**) Composites of brightfield and the maximal intensity projections of spinning disk confocal fluorescent (shown in green) micrograph stacks used to count *TgBAC(mpx:gfp)i114* neutrophils in sibling *pik3cd*$^{E525K/+}$ and *pik3cd*$^{+/+}$ 3dpf embryos. Scale bar 100μm. (**E**) Chart of neutrophils counted from single sided maximal intensity projections as in (D) for 96 sibling *pik3cd*$^{E525K/+}$ and *pik3cd*$^{+/+}$ 3dpf embryos. Bars show the mean±SEM, Mann-Whitney test. Single experiment. (**F**) Composites of brightfield and the maximal intensity projections of spinning disk confocal fluorescent (shown in green) micrograph stacks used to count *TgBAC(mpx:gfp)i114* neutrophils in sibling *pik3cd*$^{E1017K/+}$ and *pik3cd*$^{+/+}$ 2dpf embryos exposed between 24hpf and 48hpf to either 25μM CAL-101 in 1% DMSO or a 1% DMSO vehicle control. Scale bar 100μm. (**G**) Chart of neutrophils counted from single sided maximal intensity projections as in (F) for 95 sibling *pik3cd*$^{E1017K/+}$ and *pik3cd*$^{+/+}$ 2dpf embryos exposed between 24hpf and 48hpf to either 25μM CAL-101 or a DMSO vehicle control. Bars show the mean±SEM, Multiple Mann-Whitney tests. Data shown are from one experiment. Two pilot experiments with CAL-101 also showed it reduced neutrophils.

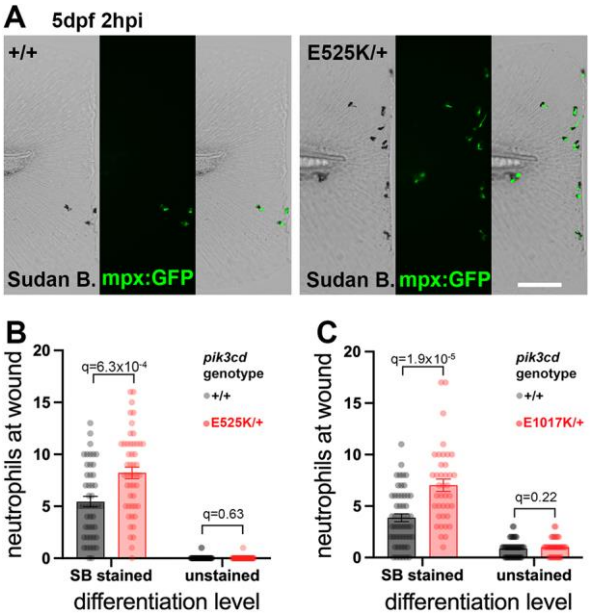

Fig. 5. Sudan black assessment of neutrophil differentiation at tail-fin injury site at 5dpf. (**A**) Brightfield and maximal intensity projection of widefield fluorescent micrographs of tail-fins of Sudan black stained, 5dpf, *TgBAC(mpx:gfp)i114*; *pik3cd*$^{E525K/+}$ and *pik3cd*$^{+/+}$ sibling embryos fixed 2hpi after transection of the tip of the tail-fin. Scale bar 100μm. (**B**) Chart of neutrophil counts at tail-fin injury site, from 96 sibling 5dpf, *pik3cd*$^{E525K/+}$ and *pik3cd*$^{+/+}$ embryos. Counts are shown both for Sudan black stained neutrophils and for those *TgBAC(mpx:gfp)i114* marked but unstained, (as in (A)). Bars show the mean±SEM, Multiple Mann-Whitney tests. Single experiment. A pilot experiment with *pik3cd*$^{E525K/+}$ also showed *TgBAC(mpx:gfp)i114* marked cells were almost all Sudan black stained. (**C**) Chart of neutrophil counts at tail-fin injury site, from 92 sibling 5dpf, *pik3cd*$^{E1017K/+}$ and *pik3cd*$^{+/+}$ embryos. Counts are shown both for Sudan black stained neutrophils and for those *TgBAC(mpx:gfp)i114* marked but unstained. Bars show the mean±SEM, Multiple Mann-Whitney tests. Single experiment.

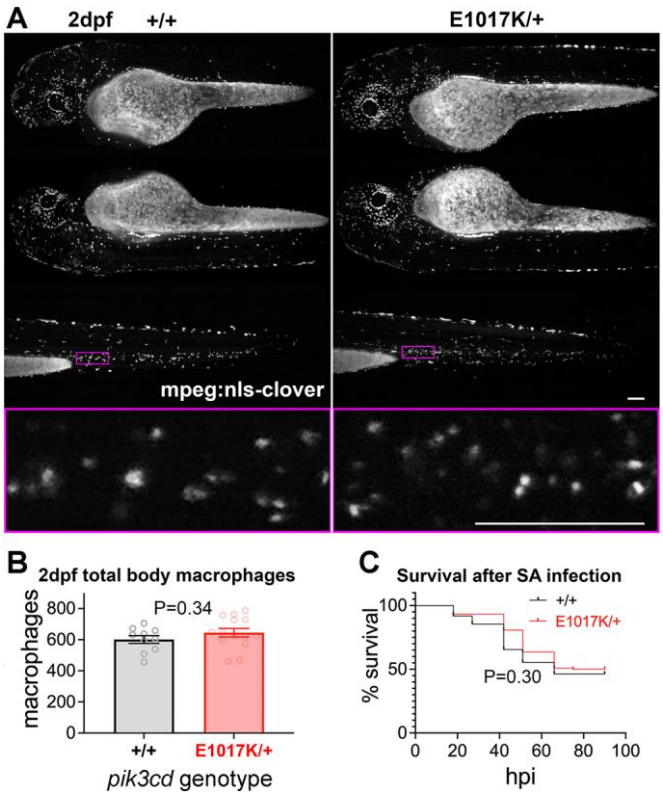

Fig. 6. Total body macrophages in *pik3cd*$^{E1017K/+}$ embryos and survival following *Staphylococcus aureus* infection. (**A**) Light sheet microscopy used to count total body *Tg(mpeg1.1:NLS-clover)sh616* macrophages of *pik3cd*$^{E1017K/+}$ and *pik3cd*$^{+/+}$ 2dpf, sibling embryos. Upper panels show maximal intensity projections for the three views used for each embryo. The magenta border shows the region displayed in lower panel as a single slice view from the image stack at higher magnification as used for counting. Scale bars 100μm. (**B**) Chart of total body macrophages counted from light sheet microscopy views as in (A) for 24 sibling 2dpf *pik3cd*$^{E1017K/+}$ and *pik3cd*$^{+/+}$ embryos. Bars show the mean±SEM, Mann-Whitney test. Single experiment. (**C**) Survival of 214 sibling *pik3cd*$^{E1017K/+}$ and *pik3cd*$^{+/+}$ embryos following injection of 1500cfu of *Staphylococcus aureus* into the circulation. Log-rank (Mantel-Cox) test. Data shown are from one experiment. A repeat experiment with 229 embryos showed similar results (P=0.99 between genotypes).

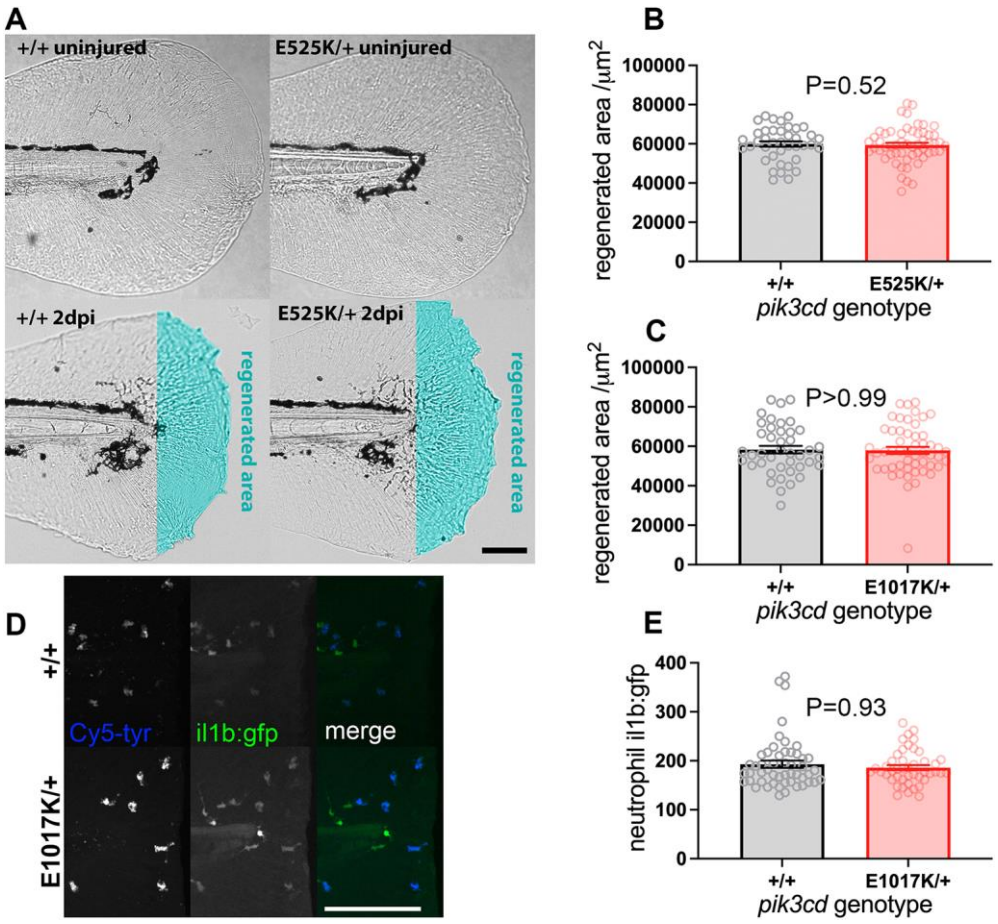

Fig. 7. Tail-fin regeneration in *pik3cd*$^{E525K/+}$ embryos. (**A**) Bright field micrographs used to measure tail-fin regeneration for *pik3cd*$^{E525K/+}$ embryos and their *pik3cd*$^{+/+}$ siblings at 5dpf, 2dpi. Upper panels show uninjured controls. Transection was through the tip of the notochord. The regenerated area is illustrated with cyan false colour. Scale bar 100µm. (**B**) Chart of tail-fin regenerated area from micrographs as in (A) for 96 embryos. Bars show the mean±SEM, Mann-Whitney test. One experiment. A similar experiment using 5dpf, 3dpi larvae also detected no effect. (**C**) Chart of tail-fin regenerated area for *pik3cd*$^{E1017K/+}$ embryos and their *pik3cd*$^{+/+}$ siblings at 5dpf, 2dpi. Measured from micrographs of 96 embryos. Bars show the mean±SEM, Mann-Whitney test. Single experiment. (**D**) Maximal intensity projections of spinning disk confocal fluorescent micrograph stacks of 3dpf *TgBAC(il1b:EGFP)sh445;pik3cd*$^{E1017K/+}$ embryos and their *pik3cd*$^{+/+}$ siblings fixed and stained 3h after tail transection. Fluorescence channels are shown for GFP and for endogenous peroxidase activity stain with Cy5-tyramide to identify neutrophils. Scale bar

100μm. (**E**) Chart of neutrophil *TgBAC(il1b:EGFP)sh445* fluorescent intensity for single neutrophils at the injury site from each of 96 3dpf sibling *pik3cd*$^{E1017K/+}$ and *pik3cd*$^{+/+}$ larvae, fixed and stained 3h after tail transection as in (D). Bars show the mean±SEM, Mann-Whitney test. Single experiment.

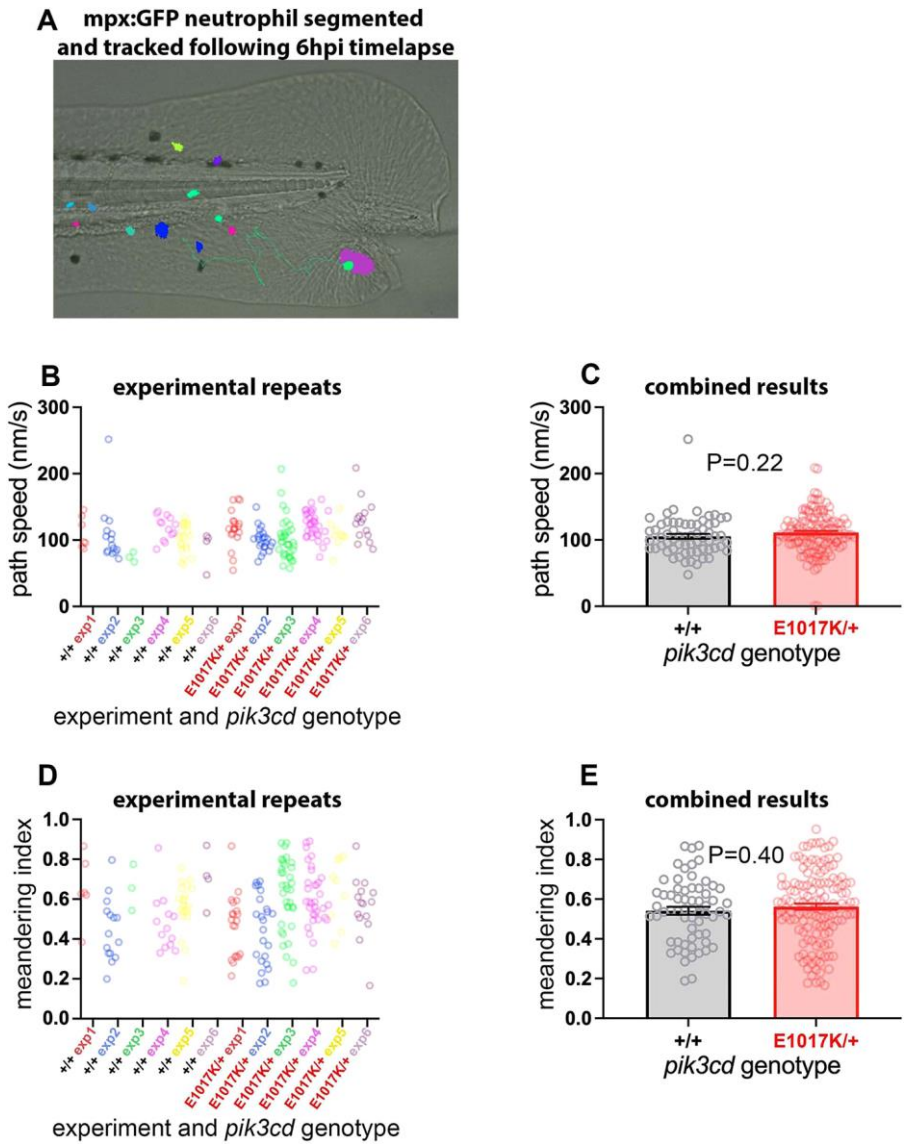

Fig. 8. Neutrophil migration in *pik3cd*$^{E1017K/+}$ embryos. (**A**) Illustrative example of the *TgBAC(mpx:gfp)i114* tail-fin injury inflammation model used to track neutrophil migration at 3dpf. Following a minor tail-fin injury and widefield time-lapse microscopy for 6hpi, semi-automated segmentation and tracking with NIS Elements software determined migration paths to the injury site. Segmented *TgBAC(mpx:gfp)i114* neutrophils are shown as false coloured patches and a migration track is shown as a green line, superimposed on a bright field micrograph (taken at the start of the time-lapse sequence). (**B**) Chart of path speeds for tracked neutrophils from sibling *pik3cd*$^{E1017K/+}$ and *pik3cd*$^{+/+}$ embryos as in (A). Data are shown for each of six experiments, each with eight or nine embryos. (**C**) Chart of pooled data from (B). Bars show the mean±SEM, unpaired t-test with Welch's correction. (**D**) Chart of meandering index (displacement/path-length) for the tracked neutrophils as in (B). (**E**) Chart of pooled data from (D). Bars show the mean±SEM, unpaired t-test with Welch's correction.

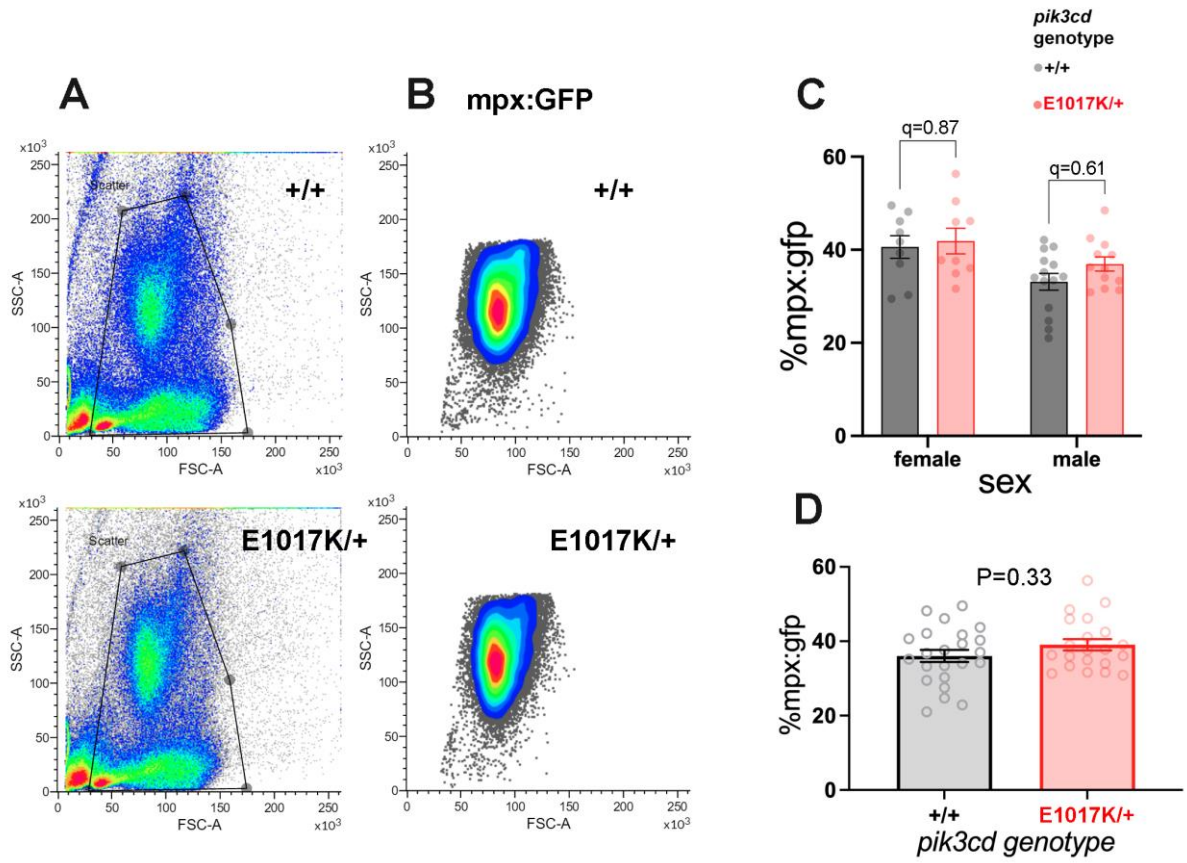

Fig. S1. Whole kidney marrow flow cytometry assessment of neutrophils in *pik3cd*$^{E1017K/+}$ adults. (A) Density plots of forward scatter and side scatter sorted whole kidney marrow from individual, eight month old, *TgBAC(mpx:gfp)i114*; *pik3cd*$^{E1017K/+}$ and *TgBAC(mpx:gfp)i114*; *pik3cd*$^{+/+}$ zebrafish. Gates are marked for the cell population analysed. (**B**) Density plots of GFP fluorescent viable cells from the cell population gated in (A). (**C**) Chart showing proportion of leukocyte and precursor cells as selected in (A) that are *TgBAC(mpx:gfp)i114* positive (as in (B)) from 21 *TgBAC(mpx:gfp)i114*; *pik3cd*$^{E1017K/+}$ and 23 *TgBAC(mpx:gfp)i114*; *pik3cd*$^{+/+}$ zebrafish, of the same age, raised together from the same clutches. Comparisons are shown for females and for males. Bars show the mean±SEM, Multiple Mann-Whitney tests. Single experiment. (**D**) The same data as in (C) but not segregated by sex. Bars show the mean±SEM, Mann-Whitney test.